February 2021

Ph.D. Thesis

Synthesis and Photophysical Investigation of Tumor-Targeted BODIPY Derivatives for Photodynamic Therapy

Chosun University Graduate School

Department of Chemistry

Vales, Temmy P.

Synthesis and Photophysical Investigation of Tumor-Targeted BODIPY Derivatives for Photodynamic Therapy

광역학치료를 위한 암-표적지향 BODIPY 유도체의 합성과 분광학적 분석

February 25, 2021

Chosun University Graduate School

Department of Chemistry

Vales, Temmy P.

Synthesis and Photophysical Investigation of Tumor-Targeted BODIPY Derivatives for Photodynamic Therapy

Supervisor Prof. Kim Ho-Joong

This thesis is submitted in partial fulfillment
of the requirements for the
Doctor of Philosophy in Chemistry

October 2020

Chosun University Graduate School

Department of Chemistry

Vales, Temmy P.

Confirmation of Doctoral's Thesis

위원장 조선대학교 교수 고 문 주 (인)

위 원 조선대학교 교수 손 홍 래 (인)

위 원 조선대학교 교수 김 호 중 (인)

위 원 조선대학교 교수 이 재 관 (인)

위 원 전남대학교 교수 조 성 (인)

December 2020

Chosun University Graduate School

TABLE OF CONTENTS

PART 3
Facile Synthesis of Mitochondria-Targeting Triphenyphosphine-Modified BODIPY Derivatives for Photodynamic Therapy

LIST OF SCHEMES

PART 2

Synthesis and Photophysical Properties of Tumor-Targeted Water-Soluble BODIPY Photosensitizers for Photodynamic Therapy

PART 3

Facile Synthesis of Mitochondria-Targeting Triphenyphosphine-Modified BODIPY Derivatives for Photodynamic Therapy

LIST OF FIGURES

PART 1
Introduction

PART 2
Synthesis and Photophysical Properties of Tumor-Targeted Water-Soluble BODIPY Photosensitizers for Photodynamic Therapy

PART 3

Facile Synthesis of Mitochondria-Targeting Triphenyphosphine-Modified BODIPY Derivatives for Photodynamic Therapy

LIST OF TABLES

PART 2

Synthesis and Photophysical Properties of Tumor-Targeted Water-Soluble BODIPY Photosensitizers for Photodynamic Therapy

LIST OF PUBLICATIONS

Seung Hwan Lee, Hoa Thi Bui, **Temmy Pegarro Vales**, Sung Cho, and Ho-Joong Kim. "Multi-color fluorescence of pNIPAM-Based nanogels modulated by dual stimuli-responsive FRET processes." Dyes and Pigments 145 (2017): 216-221.

Byungman Kang, **Temmy Pegarro Vales**, Byoung-Ki Cho, Jong-Ki Kim, and Ho-Joong Kim. "Development of gallic acid-modified hydrogels using interpenetrating chitosan network and evaluation of their antioxidant activity." Molecules 22, no. 11 (2017): 1976.

Boram Kim, Byungman Kang, **Temmy Pegarro Val**es, Si Kyung Yang, Joomin Lee, and Ho-Joong Kim. "Polyphenol-functionalized hydrogels using an interpenetrating chitosan network and investigation of their antioxidant activity." Macromolecular Research 26, no. 1 (2018): 35-39.

Temmy Pegarro Vales, Isabel Wen T. Badon, and Ho-Joong Kim. "Multi-responsive hydrogels functionalized with a photochromic spiropyran-conjugated chitosan network." Macromolecular Research 26, no. 10 (2018): 950-953.

Khuong Mai, Duy, Joomin Lee, Ilgi Min, **Temmy Pegarro Vales**, Kyong-Hoon Choi, Bong Joo Park, Sung Cho, and Ho-Joong Kim. "Aggregation-induced emission of tetraphenylethene-conjugated phenanthrene derivatives and their bio-imaging applications." Nanomaterials 8, no. 9 (2018): 728.

Bomina Shin, Jongjun Kim, **Temmy Pegarro Vales**, Si Kyung Yang, Jong-Ki Kim, Honglae Sohn, and Ho-Joong Kim. "Thermoresponsive drug controlled release from chitosan-based hydrogel embedded with poly (N-isopropylacrylamide) nanogels." Journal of Polymer Science Part A: Polymer Chemistry 56, no. 17 (2018): 1907-1914.

Se-Hee Lee, Ho-Joong Kim, Duck-Hyun Kim, Won-Seok Chang, **Temmy Pegarro Vales**, Jae-Woo Kim, Ki-Hong Kim, and Jong-Ki Kim. "Thermo-sensitive nanogel-laden bicontinuous microemulsion drug-eluting contact lenses." Journal of Biomedical Materials Research Part B: Applied Biomaterials 107, no. 4 (2019): 1159-1169.

Isabel Wen Badon , Joomin Lee, **Temmy Pegarro Vales**, Byoung Ki Cho, and Ho-Joong Kim. "Synthesis and photophysical characterization of highly water-soluble PEGylated BODIPY derivatives for cellular imaging." Journal of Photochemistry and Photobiology A: Chemistry 377 (2019): 214-219.

Duy Khuong Mai, Byungman Kang, **Temmy Pegarro Vales**, Isabel Wen Badon, Sung Cho, Joomin Lee, Eunae Kim, and Ho-Joong Kim. "Synthesis and Photophysical Properties of Tumor-Targeted Water-Soluble BODIPY Photosensitizers for Photodynamic Therapy." Molecules 25, no. 15 (2020): 3340

Temmy Pegarro Vales, Jun-Pil Jee, Won Young Lee, Ilgi Min, Sung Cho, and Ho-Joong Kim. "Protein Adsorption and Bacterial Adhesion Resistance of Cross-linked Copolymer Hydrogels Based on Poly (2-methacryloyloxyethyl phosphorylcholine) and Poly (2-hydroxyethyl methacrylate)." Bulletin of the Korean Chemical Society 41, no. 4 (2020): 406-412.

Temmy Pegarro Vales, Jun-Pil Jee, Won Young Lee, Sung Cho, Gye Myung Lee, Ho-Joong Kim, and Jung Suk Kim. "Development of Poly (2-Methacryloyloxyethyl Phosphorylcholine)-Functionalized Hydrogels for Reducing Protein and Bacterial Adsorption." Materials 13, no. 4 (2020): 943.

ACKNOWLEDGEMENT

I would like to express my sincerest gratitude to everyone who helped and supported me throughout the course of my PhD journey.

Foremost, I would like to express my special appreciation and thanks to my mentor and research supervisor, **Prof. Kim Ho-Joong**, for giving me the opportunity to study in this esteemed university, for your constant motivation and enthusiasm, for the insightful discussion, and for your endless support during the whole period of my study. Thank you, Professor Kim for allowing me to develop my own individuality and self-sufficiency by letting me work with such independence. I owe you this one, Professor!

I would like to thank my doctoral committee members, **Prof. Sohn Hong-Lae, Prof. Koh Moon Joo, Prof. Lee Jae Kwan,** and **Prof. Cho Sung**, for their invaluably constructive criticisms and comments toward improving my work.

I would like to acknowledge **Caraga State University** for granting me the study leave to pursue my dream in obtaining a PhD degree overseas.

Many thanks go to my labmates, **Isabel, Duy, Boram, Park, Seonjeong, Heejung, Eunsu, and Wookyeong** for the joy when we were together and making my PhD experience here in South Korea truly an unforgettable one. Thanks also to **Hasanul** and **Adnan,** for always lending their hands whenever I need their help.

I must express my very profound gratitude to my loving and supportive family, **Nanay Amy**, **Tatay Teddy**, **Manoy Ren-ren**, **Ate Kathy**, **Ate Elme**, **Ar-ar**, my nephews and niece, **Kier-kier**, **RJ**, **RK**, **Samuel**, and **Moses**, for their unconditional love, trust, timely encouragement, and endless patience. It was their love that raised me up again when I got weary.

Above all, where would I be without God? This accomplishment would not have been possible without His unfailing love and guidance. Life would be meaningless and nothing without Him.

ABSTRACT

Synthesis and Photophysical Investigation of Tumor-Targeted BODIPY Derivatives for Photodynamic Therapy

Temmy P. Vales
Advisor: Prof. Kim, Ho-Joong, Ph.D.
Department of Chemistry
Graduate School of Chosun Unicersity

We reported the synthesis of three lactose-functionalized 4,4-difluoro-4-bora-3a,4a-diaza-s-indacene (BODIPY)-based dyes capable of targeting cancer cells and investigated their photodynamic therapeutic property on three distinct malignant cell lines (breast cancer MCF-7 cell lines, cervical cancer HeLa, and human hepatoma Huh7). The halogenation of BODIPY dyes has resulted to a decreased fluorescence quantum yield and effectively facilitated the high production of singlet oxygen species. The synthesized BODIPY derivatives demonstarted low cytotoxicities in the dark and high photodynamic therapeutic capabilities against the treated cancer cell lines after LED irradiation. Furthermore, the modification with the lactose and triphenylphosphine groups resulted to an increased cellular uptake of the BODIPY dyes. In summary, the results presented herein signify the promising potentials of BODIPY dyes as photodynamic therapeutic agents for cancer treatment.

PART 1
INTRODUCTION

1.1. General features and synthesis of the parent BODIPY core

The first report involving the difluoro-boraindacene family [4,4-difluoro-4-bora-3a,4a-diaza-s- indacene (BODIPY)] originated in 1968 when Treibs and Kreuzer noticed that the reaction between acetic anhydride and 2,4- dimethylpyrrole, in the presence of boron trifluoride as Lewis acid catalyst, generated a highly fluorescent BODIPY compound, instead of the desired acylated pyrroles as shown in Figure 1.1 [1].

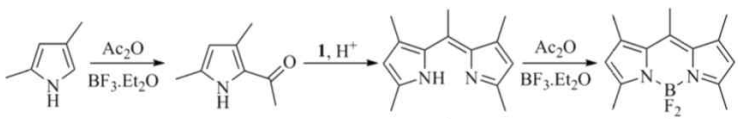

Figure 1.1. First synthesis of a BODIPY dye [1].

The BODIPY and its derivatives are generally highly colored and show intense absorption and emission profiles (λ_{max} between 500-545 nm). Moreover, these dyes possess outstanding photophysical features, when compared to that of the classical fluorophores such as tetramethylrhodamines and fluorescein dyes, including high fluorescence quantum yields (normally Φ_F > 0.60), high molar absorption coefficients (typically in the region of 40,000 to 80,000 M^{-1} cm^{-1}), reasonably long fluorescence lifetimes (τ in the nanosecond range) and

relatively small Stokes shift (ca.10 nm). Furthermore, BODIPY-based derivatives are thermal and photostable in both solid and solution states, insensitive to any change in pH and solvent polarity, and can be dissolved in most organic solvents. [2-4]. These advantageous characteristics combine with a low toxicity [5], enable the BODIPY dyes to be used for several biological applications as bioimaging agents, probes, photosensitizers, and among others [6-8].

The numbering of the BODIPY systems according to the International Union of Pure and Applied Chemistry (IUPAC) is depicted in Figure 1.2. In spite of the similarity in the structures with the dipyrromethane and dipyrrin molecules, the boron complex is numbered differently. The central carbon, as in the case for all three compounds, is designated as the meso position, stemming from the nomenclature of porphyrin. Moreover, the carbon adjacent to the nitrogen atoms are referred to as α-carbon, suggesting the peculiar reactivity of this carbon in pyrroles, while the others are called β-carbons [9].

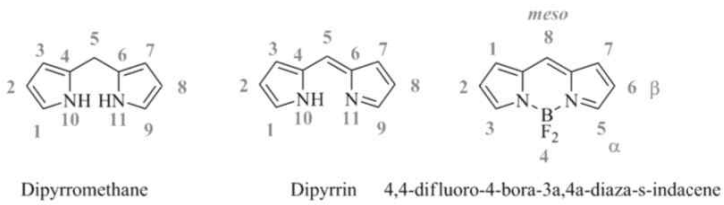

Figure 1.2. IUPAC numbering of a dipyrromethane, a dipyrrin, and a BODIPY molecule [9].

There are two most common synthetic routes to the BODIPY core, and both of them are anchored on the chemistry well known from porphyrin research. The first approach, as illustrated in Figure 1.3a, involves the acid catalyzed condensation of aldehydes with pyrrole to afford an unstable dipyrromethane. The subsequent oxidation of dipyrromethane, using either 2,3-Dichloro-5,6-dicyano-1,4-benzoquinone (DDQ) or p-chloranil, results to a dipyrromethene, or dipyrrin. Reacting the dipyrrin to the boron trifluoride etherate in the presence of a base finally affords the BODIPY core in high yields [9]. The second

synthetic route involves condensation of pyrrole with an acylium equivalent (Figure 1.3b). The acylium equivalent employed are either an acid chloride [10], anhydride [11] or an orthoester [12]. In this approach, an intermediate acylpyrrole is usually not isolated since it can directly form a dipyrrin with an excess of pyrrole. Similar to the first approach, subjecting the dipyrrin with an excess of base and boron trifluoride etherate generates the BODIPY dye. Furthermore, the second route is more advantageous as it allows the synthesis of asymmetric BODIPY dyes since the dipyrrins, as an isolated acylpyrrole, can react with a second pyrrole molecule in an acidic condensation.

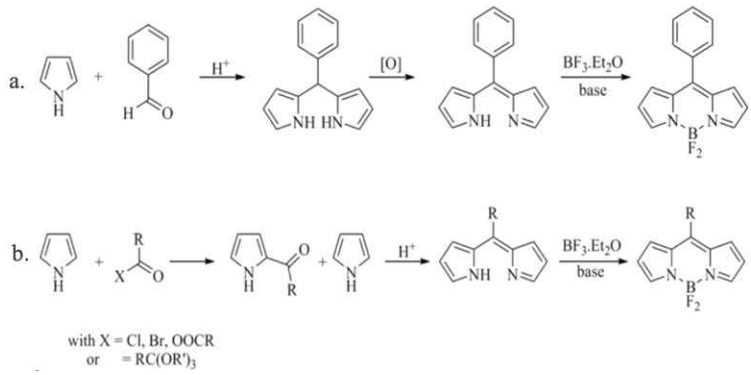

Figure 1.3. (a) Synthesis of BODIPY dye via acid-catalyzed condensation of an aromatic aldehyde with pyrrole. (b) Synthesis of BODIPY dye via acid-catalyzed condensation of an acylpyrrole with another pyrrole molecule.

1.2. Functionalization *via* the meso substituent

The functionalization *via* the meso substituent has been regarded as the most versatile approach for the introduction of several groups on the BODIPY core including donor-acceptor groups [13], ligands [14,15], and water-soluble moieties [4,16]. This results to a wide-array of BODIPY derivatives for various applications as photosensitizers, probes, biological labels, and sensors [6-8] (Figure 1.4). Furthermore,

the easy process of functionalization at the C-8 (meso) position makes it more advantageous relative to that of the substitution at the pyrrolic positions, since the process can be readily achieved via acid-catalyzed condensation of pyrrole with suitably substituted aryl aldehydes or acyl chlorides [17].

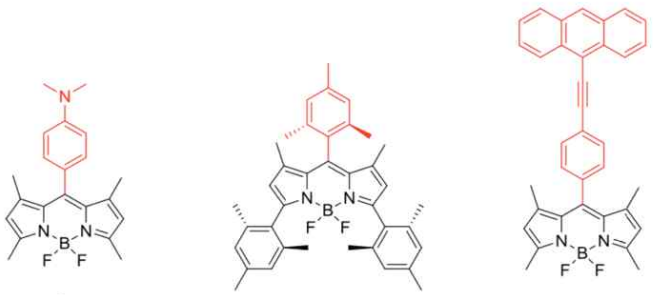

Figure 1.4. Chemical structures of several *meso*-substituted BODIPY dyes reported in the literature [6-8].

Boens and co-workers have conducted in-depth photophysical studies on the effect of various electron-donating or electron-withdrawing moieties at the meso positions [18-20]. There has been no marked change in the spectral characteristics of 8-substituted BODIPYs. This could be attributed to the orthogonal geometry between the meso group and BODIPY core, resulting to a poor electronic conjugation between the two moieties. However, restricted intramolecular rotation and steric hindrance between the substituents could drastically improve the fluorescence emission efficiency. This can be achieved by introducing ortho-substituents on the meso-phenyl ring, replacing phenyl with bulkier aromatic groups or introducing substituents to 1,7-positions on the BODIPY skeleton [21].

The exchange of C-meso for nitrogen atom results to another sub-class of BODIPY dye referred to as “aza-BODIPYs” (Figure 1.5). The aza-BODIPYs were found to have improved stability and superior spectral properties in comparison to their carbon analogues due to the

further rigidification of the chromophoric core. Particularly, the absorption and emission maxima of aza-BODIPYs were found to be red-shifted (absorption and emission bands in the 650-850 nm range), which could be attributed to the greater stabilization of the HOMO-LUMO energy gap by lone pair on nitrogen at the meso position. Several aza-BODIPYs have been synthesized from substituted-chalcone [22-24] or from a conformationally restricted pyrrole precursor [25]. These dyes were investigated as imaging probes [22,24], fluorescent labels for polymer characterization [26], and photosensitizers [27].

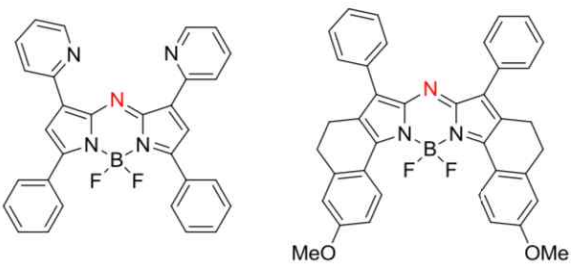

Figure 1.5. Chemical structures of several aza-BODIPY dyes reported in the literature [22,24].

1.3. Halogenated BODIPY dyes

A closer look at the mesomeric structures of BODIPY, as indicated in Figure 1.6, shows that the carbons at 2- and 6-positions of the BODIPY core possess the least positive charge and are more susceptible to be attacked by the electrophiles. There have been few reported electrophilic substitution reactions at the 2,6-positions into the BODIPY core via the electron-rich 2,6-carbons including sulfonation [28], nitration [29], formylation [30], and halogenation [31].

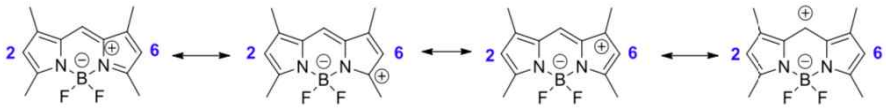

Figure 1.6. Mesomeric structures of BODIPY dye indicating the positions susceptible to electrophilic attack.

In particular, a significant attention has been given to the synthesis of halogenated BODIPY derivatives since these dyes paved a way to a wide range of reactions available for halogenated aromatic heterocycles. For instance, a monoiodinated BODIPY dye was synthesized via condensation reaction between 4-iodo-3,5-dimethyl-2-pyrrolecarboxaldehyde and dimethylpyrrole. This monoiodinated dye has been an excellent scaffold for palladium catalyzed Sonogashira coupling reaction as demonstrated in Figure 1.7 [32].

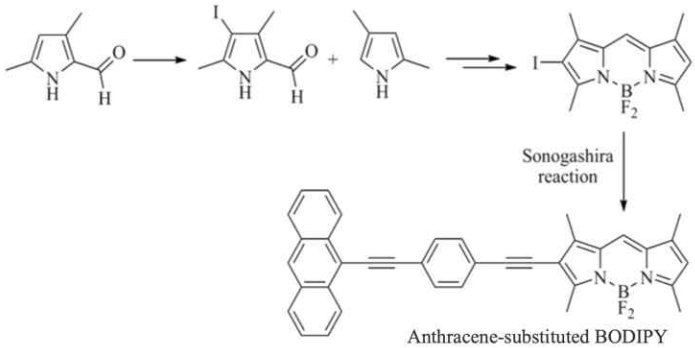

Figure 1.7. Synthesis of an anthracene-substituted BODIPY dye via halogenation of a pyrrole followed by Palladium-catalyzed Sonogashira coupling reaction [32].

In addition, iodination reaction has been employed as a means to shut down fluorescence and induce production of triplet state. These triplet states could then be employed for photodynamic therapy (PDT)

via generation of singlet oxygen, a highly reactive and toxic oxygen species that can induce irreversible damages to malignant cells. As shown in Figure 1.8, the diiodination of a BODIPY dye has resulted in a derivative with quenched fluorescence and high efficiency as photosensitizer for PDT application [29].

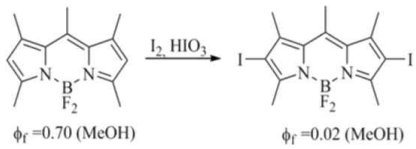

Figure 1.8. Halogenated BODIPY photosensitizer with quenched fluorescence quantum yield [29].

1.4. Research outlook

In spite of the several advancements in the field of BODIPY research, these dyes are far from being mature. The dyes' inherent insolubility to the aqueous media and the lack of targeting capability remain the long-standing challenges in the BODIPY biomarker community. With these facts in mind, the synthesis, photophysical characterization and photodynamic therapeutic assessment of the water-soluble, tumor-targeted BODIPY dyes will be discussed in the next Chapters.

1.5. References

[1] Treibs, A.; Kreuzer, F.H. *Justus Liebigs Annalen der Chemie*. **1968**, 718, 208-223.

[2] Loudet, A.; Burgess, K. *Chemical reviews*, **2007**, *107*, 4891-4932.

[3] Li, L.; Nguyen, B.; Burgess, K. *Bioorganic & medicinal chemistry letters*, **2008**, *18*, 3112-3116.

[4] Thivierge, C.; Bandichhor, R.; Burgess, K. Organic letters, **2007**, 9, 2135-2138.

[5] Alford, R.; Simpson, H.M.; Duberman, J.; Hill, G.C.; Ogawa, M.; Regino, C.; Kobayashi, H.; Choyke, P.L. *Molecular imaging*, **2009**, *8*, 7290-2009.

[6] Baruah, M.; Qin, W.; Basarić, N.; De Borggraeve, W.M.; Boens, N. *The Journal of organic chemistry*, **2005**, *70*, 4152-4157.

[7] Zaitsev, A.B.; Méallet-Renault, R.; Schmidt, E.Y.; Al'bina, I.M.; Badré, S.; Dumas, C.; Vasil'tsov, A.M.; Zorina, N.V.; Pansu, R.B. *Tetrahedron*, **2005**, *61*, 2683-2688.

[8] Wan, C.W.; Burghart, A.; Chen, J.; Bergström, F.; Johansson, L.B.Å.; Wolford, M.F.; Kim, T.G.; Topp, M.R. Hochstrasser, R.M.Burgess, K. *Chemistry-A European Journal*, **2003**, *9*, 4430-4441.

[9] Wood, T.E.; Thompson, A. *Chemical reviews*, **2007**, *107*, 1831-1861.

[10] Boyer, J.H.; Haag, A.M.; Sathyamoorthi, G.; Soong, M.L.; Thangaraj, K.; Pavlopoulos, T.G. *Heteroatom Chemistry*, **1993**, *4*, 39-49.

[11] Li, Z.; Mintzer, E.; Bittman, R. *The Journal of organic chemistry*, **2006**, *71*, 1718-1721.

[12] Yakubovskyi, V.P.; Shandura, M.P.; Kovtun, Y.P. European Journal of Organic Chemistry, **2009**, 2009, 3237-3243.

[13] Zrig, S.; Rémy, P.; Andrioletti, B.; Rose, E.; Asselberghs, I.; Clays, K. The Journal of organic chemistry, **2008**, 73, 1563-1566.

[14] Ulrich, G.; Ziessel, R. The Journal of organic chemistry, **2004**, 69, 2070-2083.

[15] Ulrich, G.; Ziessel, R.; Harriman, A. Angewandte Chemie International Edition, **2008**, 47, 1184-1201.

[16] Ntziachristos, V.; Bremer, C.; Weissleder, R. *European radiology*, **2003**, *13*, 195-208.

[17] Jiao, L.; Yu, C.; Li, J.; Wang, Z.; Wu, M.; Hao, E. *The Journal of organic chemistry*, **2009**, *74*, 7525-7528.

[18] Boens, N.; Leen, V.; Dehaen, W. *Chemical Society Reviews*, **2012**, *41*, 1130-1172.

[19] Baruah, M.; Qin, W.; Flors, C.; Hofkens, J.; Vallee, R.A.; Beljonne, D.; Van der Auweraer, M.; De Borggraeve, W.M.; Boens, N. T*he Journal of Physical Chemistry A*, **2006**, *110*, 5998-6009.

[20] Baruah, M.; Qin, W.; Basarić, N.; De Borggraeve, W.M.; Boens, N. *The Journal of organic chemistry*, **2005**, *70*, 4152-4157.

[21] Hu, R.; Lager, E.; Aguilar-Aguilar, A; .Liu, J.; Lam, J.W.; Sung, H.H.;

Williams, I.D.; Zhong, Y.; Wong, K.S.;Pena-Cabrera, E.; Tang, B.Z. *The Journal of Physical Chemistry C*, **2009**, *113*, 15845-15853.

[22] Loudet, A.; Bandichhor, R.; Burgess, K.; Palma, A.; McDonnell, S.O.; Hall, M.J.; O'Shea, D.F. *Organic letters*, **2008**, *10*, 4771-4774.

[23] Coskun, A.; Yilmaz, M.D.; Akkaya, E.U. *Organic Letters*, 2007, *9*, 607-609.

[24] Loudet, A.; Bandichhor, R.; Wu, L.; Burgess, K. *Tetrahedron*, **2008**, *64*, 3642-3654.

[25] Zhao, W.; Carreira, E.M., *Angewandte Chemie*, **2005**, *117*, 1705-1707.

[26] Yoshii, R.; Nagai, A.; Chujo, Y. J*ournal of Polymer Science Part A: Polymer Chemistry*, **2010**, *8*, 5348-5356.

[27] Adarsh, N.; Avirah, R.R.; Ramaiah, D. *Organic Letters*, **2010**, *12*, 5720-5723.

[28] Wories, H.J.; Koek, J.H.; Lodder, G.; Lugtenburg, J.; Fokkens, R.; Driessen, O.; Mohn, G.R. *Recueil des Travaux Chimiques des Pays-_Bas*, **1985**, *104*, 288-29.

[29] Pavlopoulos, T.G.; Boyer, J.H.; Shah, M.; Thangaraj, K.; Soong, M.L. A*pplied optics*, **1990**, *29*, 3885-3886.

[30] Jiao, L.; Yu, C.; Li, J.; Wang, Z.; Wu, M.; Hao, E., *The Journal of organic chemistry*, **2009**, *74*, .7525-7528.

[31] Haugland, R.P.; Kang, H.C. Molecular Probes Inc, C*hemically reactive dipyrromethene*b*oron difluoride dye*s. **1988**, U.S. Patent 4,774,339.

[32] Zhao, W.; Carreira, E.M. *Chemistry-A European Journal*, **2006**, *12*, 7254-7263.

PART 2

Synthesis and Photophysical Properties of Tumor-Targeted Water-Soluble BODIPY Photosensitizers for Photodynamic Therapy

2.1. Introduction

Photodynamic therapy (PDT) is a noninvasive cancer treatment that employs three nontoxic components: a photosensitizing (PS) agent, oxygen and light [1,2]. PDT's mode of action relies on the generation of highly reactive oxygen species (ROS), including singlet oxygen ($^1O_2$), following irradiation of the localized photosensitizers with light of appropriate wavelengths. This eventually causes irreversible damage in the regions where these three key components converge [3]. Numerous photosensitizers have been reported for use in PDT, such as cyclic tetrapyrroles (chlorins, porphyrins, and bacteriochlorins) and phenothiazinium-based photosensitizers [4-7]. However, the majority of these PS agents suffers from several setbacks including low photostability, low light-to-dark toxicity ratios, and structural instability, resulting to the dyes' confined clinical applications. Furthermore, elaborative synthetic processes are generally employed to synthesize these conventional PS agents and can only be used with a limited number of solvents [8-10]. Hence, there is an avenue to develop new classes of PDT photosensitizers that are straightforward to synthesize, highly efficient, photostable, and widely applicable under

various conditions.

A promising class of fluorophore that has shown excellent potential as a PS agent over the past decade is 4,4-difluoro-4-bora-3a,4a-diaza-s-indacene (BODIPY) [7,11-13]. A greater attention has been given to this class of dyes not only in fundamental research but also in clinical practice. This is attributed to its intrinsic superior photophysical characteristics including high extinction coefficients, high fluorescence quantum yield, resistance to photobleaching [11,14], and high light-to-dark toxicity ratios, which are higher than those of conventional phenothiazinium-based PDT agents [2,5]. Furthermore, these dyes are amenable to several post-synthetic modifications focused on improving their photophysical characteristics and ROS generation efficiency. In particular, the addition of heavy halogen atoms at the 2,6-positions of the BODIPY chromophore could significantly increase singlet-to-triplet intersystem crossing (ISC) transitions of the chromophore and subsequently increase the production of $^1O_2$. Such modification with heavy atoms onto a molecule that significantly influences the rates of ISC is referred to as the heavy-atom effect [15]. Despite the significant advances in BODIPY biomarker research, only few BODIPY derivatives have found their biological utility since most of the synthesized BODIPY dyes are inherently hydrophobic, not sufficiently selective toward tumor cells, and prone to form aggregates in aqueous media [16-18]. Several synthetic methodologies have been reported for increasing the tumor-selectivity and aqueous solubility of these PS agents, including the attachment of ionizable hydrophilic groups (e.g., sulfonic acid, carboxylic acid, phosphonic acid, and ammonium groups), and biomolecules (e.g., polyethylene glycol, oligonucleotides, and carbohydrates) [19-21].

Among the multitude of ionizable hydrophilic groups and biomolecules used to enhance the water solubility of BODIPY derivatives, carbohydrate groups have shown an exceptional capability in balancing the biocompatibility, stability, biodegradability, and tumor-targeting efficacy of the resulting photosensitizers [22]. It is well established that carbohydrates play a significant role in cellular recognition

processes and are considered crucial signaling molecules [23]. Carbohydrate-functionalized photosensitizers are thought to possess a remarkable potential in cancer treatment due to their enhanced interactions with several overexpressed specific receptors in tumor cells via carbohydrate-mediated cell recognition processes [24,25]. In particular, lactose, a disaccharide compose of galactose and glucose units, has been considered as a promising targeting ligand for photodynamic therapeutic applications. In an aqueous medium, the glucose moiety transforms into its chain structure, while the galactose group remains in a stable ring structure [26]. Recent developments in the field of molecular recognition have shown the targeting capabilities of the galactose moiety and lactose-functionalized macromolecules against numerous human malignant cells, particularly hepatocellular carcinoma cells [27-30].

Despite sophisticated carbohydrate-based synthetic approaches designed by glycoscientists [31,32], the development of an effective synthetic methodology that is straightforward, versatile, rapid, regiospecific, high-yielding, and does not involve complicated purification processes remains desirable, to compliment the ever-growing importance in the preparation of functional carbohydrate-based macromolecules. Due to the aforementioned exceptional features, a wide range of BODIPY-carbohydrate functional materials have been developed and found wide applications in the fields of biology, chemistry, and material science [33-35]. Herein, we reported the synthesis of a series of BODIPY-based photosensitizers conjugated with a lactose moiety that are tumor-targeting capable and water soluble via the copper iodide (CuI) catalyzed azide-alkyne cycloaddition (CuAAC) click reaction. Extensive photophysical investigations including UV/Vis absorbance and emission, fluorescence quantum yield, and singlet oxygen quantum yield measurements were performed to the synthesized BODIPY derivatives. Moreover, the assessment of the photodynamic therapeutic properties and biocompatibilities of the synthesized BODIPY derivatives was carried out against three distinct malignant cell lines (breast cancer MCF-7 cell lines, cervical cancer HeLa, and human hepatoma Huh7).

2.2. Materials and Methods

2.2.1. Materials

All reagents were obtained from commercial sources. Acetic anhydride, *N*,*N*-dimethylformamide (DMF), D-lactose, trichloroacetonitrile, propargyl alcohol, *N*-iodosuccimide (NIS), 1,8-diazabicyclo [5.4.0]undec-7-ene (DBU), sodium metal, 5-bromovaleryl chloride, boron trifluoride diethyl etherate ($BF_3 \cdot Et_2O$), 2,4-dimethyl pyrrole, Dowex-50 resin (H^+ form), and triethylamine (TEA) were procured from Sigma Aldrich (St. Louis, MO, USA). Copper (II) sulfate pentahydrate, sodium azide, sodium hydroxide (NaOH), sodium ascorbate, sodium hydrogen carbonate ($NaHCO_3$), sulfuric acid (H_2SO_4), ammonium carbonate [$(NH_4)_2CO_3$], and magnesium sulfate ($MgSO_4$) were purchased from Daejung Chemical (Gyeonggi-do, South Korea) and used without further purification. Methanol, ethyl acetate (EtOAc), tetrahydrofuran (THF) dichloromethane (CH_2Cl_2), and other solvents were of analytical grade and were dried under calcium hydride prior to use, except THF. All compounds were characterized by ^1H- and ^{13}C-NMR spectroscopy on a Bruker AM 250 spectrometer (Billerica, MA, USA) and high-resolution electrospray ionization mass spectrometry (HR-ESI-MS) on a SYNAPT G2-Si high definition mass spectrometer (Waters, London, United Kingdom).

2.2.2. Synthesis of Lactose-Modified Water Soluble BODIPY Derivatives

2.2.2.1. Synthesis of the BODIPY Core

The BODIPY core was synthesized in accord to our previously reported

literature [36]. In a 250-mL dry, round-bottomed flask, 2,4-dimethyl pyrrole (1.75 mL, 17.04 mmol) and 5-bromovaleryl chloride (1.14 mL, 8.52 mmol) were dissolved in dry CH_2Cl_2 (100 mL) at room temperature, degassed with a stream of Ar gas for 2 min, and refluxed for 2 h. The solvents were then evaporated on a rotary evaporator. The residual mixture was re-dissolved in a mixture of toluene and CH_2Cl_2 (10:1, *v*/*v*), added with TEA (4.8 mL) and $BF_3 \cdot Et_2O$ (4.2 mL), and heated at 50 ° C. After 1.5 h the solvents were evaporated *in vacuo* and the crude product was purified via column chromatography to afford the BODIPY core as an orange solid (2.12 g, 65% yield).

^{1}H-NMR (300 MHz, $CDCl_3$, δ, ppm): 6.07 (s, 2H), 3.48-3.43 (t, 2H), 3.02-2.96 (t, 2H), 2.52 (s, 6H), 2.43 (s, 6H), 2.08-2.04 (m, 2H), 1.87-1.82 (m, 2H).

2.2.2.2. Synthesis of Dye 1

The previously synthesized BODIPY core (120 mg, 0.313 mmol) was dissolved in DMF (10 mL) under Ar gas and subsequently added with NaN_3 (407 mg, 6.2 mmol). The mixture was then stirred at room temperature for 20 h. The resulting mixture was extracted with CH_2Cl_2 and washed successively with water and brine. The obtained organic phases were combined, dried over $MgSO_4$, filtered and the solvent removed in vacuo. Column chromatographic purification was performed to the crude product affording the BODIPY dye 1 as a bright-orange solid (102 mg, 94% yield).

^{1}H-NMR (300MHz, $CDCl_3$, δ, ppm): δ 6.07 (s, 2H), 3.39-3.35 (t, 2H), 3.01-2.95 (t, 2H), 2.52 (s, 6H), 2.42 (s, 6H), 1.78-1.75 (m, 4H).

2.2.2.3. Synthesis of BODIPY Dyes 2a and 2b

BODIPY dye 2a and 2b were synthesized according to our previously described procedure [37]. A representative procedure is indicated for BODIPY dye 2a. Briefly, BODIPY dye 1 (300 mg, 0.87 mmol) was dissolved in dried CH_2Cl_2. The resulting misture was added with NIS (117 mg, 0.52 mmol) and stirred at room temperature. After 2 h, the solvent was evaporated on a rotary evaporator. The crude product was purified by column chromatography to afford BODIPY dye 2a as an orange solid (319 mg, 78% yield).

^{1}H-NMR (300MHz, $CDCl_3$, δ, ppm): δ 6.13 (s, 1H), 3.47-3.43 (t, 2H), 3.01-2.97 (t, 2H), 2.60 (s, 3H), 2.53 (s, 3H), 2.46 (s, 3H), 2.43 (s, 3H), 2.08-2.03 (m, 2H), 1.84-1.79 (m, 2H).

The di-iodinated BODIPY Dye 2b was synthesized in the same manner as the mono-iodinated BODIPY dye 2a, except that the NIS equivalents were doubled. The BODIPY dye 2b was obtained as a red solid (85% yield).

^{1}H-NMR (300MHz, $CDCl_3$, δ, ppm): δ 3.49-3.44 (t, 2H), 3.08-3.03 (t, 2H), 2.62 (s, 6H), 2.50 (s, 6H), 2.10-2.05 (m, 2H), 1.86-1.78 (m, 2H).

2.2.2.4. General Procedure for the Preparation of Water-Soluble Dyes BLa, BILa, and BDILa

A series of water-soluble BODIPY dyes BLa, BILa, and BDILa was prepared in accord to our previously reported procedure [38]. A representative procedure is shown for BLa.

BLa: BODIPY dye 1 (55 mg, 0.16 mmol), lactose propargyl (67 mg, 0.175 mmol), NaAsc (158 mg, 0.797 mol), and $CuSO_4.5H_20$ (80 mg, 0.32 mmol) were dissolved in a mixture of THF/water (15/5 mL, *v*/*v*) and the resulting mixture was stirred for 24 h at room temperature. The crude mixture was extracted with EtOAc and water three times. The organic phases were collected, combined, and dried over $MgSO_4$. Following filtration and solvent removal on a rotary evaporator, the product was recrystallized from MeOH/diethyl ether to obtain a black-red solid (yield 60 mg, 52% yield).

^{1}H-NMR (300 MHz, $CDCl_3$, δ, ppm): δ 8.05 (s, 1H), 6.14 (s, 2H), 4.52-4.5 (t, 2H), 4.44-4.39 (m, 2H), 3.96-3.94 (m, 2H), 3.84-3.78(m, 4H), 3.76-3.73 (m, 2H), 3.70-3.67 (m, 4H), 3.61-3.58 (t, 2H), 3.05-3.03 (m, 2H), 2.45 (s, 6H), 2.39 (s, 6H), 1.64-1.61 (m, 4H)

^{13}C-NMR (75 MHz, CD_3OD, δ, ppm): 155.02, 146.86, 145.43, 142.22, 132.39, 125.46, 122.53, 104.87, 103.47, 80.57, 77.02, 76.1, 74.72, 74.38, 72.37, 70.07, 63.2, 62.26, 61.8, 55.03, 50.29, 32.71, 31.33, 30.7, 28.55, 23.64, 16.4, 14.26

HR-MS-ESI: *m*/*z* 748.3154, calcd mass for $C_{32}H_{46}N_5O_{11}NaBF_2$ 748.3153

BILa: The BODIPY dye BILa was synthesized according to the above-detailed general procedure to obtain the title product as an orange solid (47% yield).

^{1}H-NMR (300 MHz, $CDCl_3$, δ, ppm): δ 8.03 (s, 1H), 6.21 (s, 1H), 4.45-4.43 (t, 2H), 4.4-4.39 (m, 2H), 3.97-3.94 (m, 2H), 3.86-3.81 (m, 4H), 3.75-3.74 (m, 2H), 3.63-3.58 (m, 4H), 3.47-3.46 (t, 2H), 2.88-2.87 (t, 2H), 2.53 (s, 3H), 2.48 (s, 3H), 2.3 (s, 6H), 2.08-2.07 (m, 2H), 1.56-1.55 (m, 2H)

^{13}C-NMR (75 MHz, CD_3OD, δ, ppm): 164.92, 157.84, 153.67, 146.95, 145.64, 144.75, 141.76, 133.13, 131.89, 125.53, 124.11, 105.05, 103.47, 80.69, 77.0, 76.49, 76.25, 74.74, 72.47, 70.32, 63.1, 62.46, 61.92, 50.71, 31.65, 31.27, 29.52, 28.59, 18.73, 16.74, 14.8

HR-MS-ESI: *m/z* 874.2120, calcd mass for $C_{32}H_{45}N_5O_{11}NaBF_2I$ 874.2119

BDILa: The BODIPY dye BDILa was synthesized according to the above-detailed general procedure to obtain the title product as a red solid (63% yield).

^{1}H-NMR (300 MHz, $CDCl_3$, δ, ppm): δ 8.05 (s, 1H), 4.43-4.41 (t, 2H), 4.38-4.36 (m, 2H), 3.91-3.8 (m, 5H), 3.78-3.76 (m, 2H), 3.7-3.66 (m, 5H), 3.47-3.44 (t, 2H), 3-2.88 (t, 2H), 2.55 (s, 2H), 2.39 (s, 6H), 2.14-2.1 (m, 2H), 1.61-1.59 (m, 2H)

^{13}C-NMR (75 MHz, CD_3OD, δ, ppm): 156.35, 147.21, 145.71, 144.12, 132.46, 126.1, 125.53, 105.13, 103.55, 101.87, 98.1, 93.72, 80.63, 77.02, 76.52, 76.28, 74.75, 73.16, 72.62, 71.31, 70.36, 62.47, 61.91, 56.58, 50.3, 32.12, 29.48, 27.8, 23.6, 19.24, 16.35, 14.42

HR-MS-ESI: *m/z* 1000.1086, calcd mass for $C_{32}H_{44}N_5O_{11}NaBF_2I_2$ 1000.1085

2.2.3. Measurement of Photophysical Properties

UV absorption spectra were recorded in a 1-cm path length quartz cuvette employing a double-beam UV-2800 Uv-vis spectrophotometer (Shimadzu, Kyoto, Japan) at room temperature. The steady-state emission

spectra were acquired using a F-4500 steady-state fluorometer (Hitachi, Tokyo, Japan) with an Xenon arc lamp and a photomultiplier detection system. All spectra were measured at 300-700 nm, in triplicate, and corrected for background intensities by subtracting the spectra of pure solvent measured under identical conditions.

2.2.4. Fluorescence Quantum Yield Measurements

The relative fluorescence quantum yields of BODIPY BLa, BILa, and BDILa were obtained by comparing the area under the corrected emission spectrum of the samples with that of a standard solution with a known fluorescence quantum yield. Herein, Rhodamine 6G was used as the reference standard, which possesses a known quantum yield of 0.94 in methanol [39]. The Φ_f was calculated according to equation below:

$$\Phi_S = \Phi_R \left(\frac{Grad_S}{Grad_R}\right)\left(\frac{n_S}{n_R}\right)^2$$

where the subscripts S and R represent the tested sample and reference, respectively. In addition, Grad and n denote the gradient of the filled slope and the refractive index of the test solvent used, respectively. The solutions were optically diluted to avoid inner filter effects [40].

2.2.5. Singlet Oxygen Quantum Yield

The sample quantum yields of singlet oxygen (Φ_Δ) were studied using 1,3-diphenylisobenzofuran (DBPF) as a chemical quencher [41]. Briefly, a mixture of each BODIPY dye (absorption ~0.06 at 524 nm in EtOH) and DPBF (absorption ~1.0 at 424 nm in EtOH) was irradiated with

a green LED lamp (λ_{max} = 500 nm). The photooxidation of DPBF was then monitored between 0 and 70 min, depending on the efficiency of the BODIPY dye. The singlet oxygen quantum yield was calculated using hematoporphyrin (HP) as the reference, with a yield of 0.53 in ethanol, according to the following equation:

$$\Phi_{\Delta}^{S} = \frac{k_S}{k_R} \times \Phi_{\Delta}^{R}$$

where subscripts S and R represent the sample and reference, respectively, while k represents the slope of the photodegradation rate.

2.2.6. Cells and Cultures

The three cancer cell lines, namely human cervix adenocarcinoma (HeLa), human breast adenocarcinoma (MCF-7), and hepato liver carcinoma (Huh7), were obtained from Korean Cell Line Bank and maintained according to the provider's instructions. Briefly, the cell lines were cultured under standard culture conditions (5% CO_2 and 95% air at 37 °C) in an RPMI 1640 medium (Gibco, Carlsbad, CA, USA) supplemented with 10% heat-inactivated fetal bovine serum (FBS) and antibiotic (100 U/mL penicillin and 100 mg/mL streptomycin) (WELGENE Inc., Gyeongsangbuk-do, Korea).

2.2.7. Photodynamic Anticancer Activity Assessment

HeLa, MCF-7 and Huh7 cells were seeded in 96-well plates (3×10^3 cells/well). The cells were maintained for 24 h and treated with a

range of test compound concentrations (0, 0.25, 0.5, 1.0 and 2.0 μM) for 24 h [42,43]. A cell proliferation assay was measured via CellTiter 96® AQueous one solution cell proliferation assay (Promega, Madison, WI, USA) according to the manufacturer's instructions. The absorbance was determined at 490 nm using an enzyme-linked immunosorbent assay (ELISA) plate reader (Thermo Fisher Scientific, Inc., Waltham, MA, USA).

2.2.8. Cell Proliferation Assay

Pre-cultured cancer cells were plated at 3 × 10^3 cells/well in a 96-well plate and incubated at 37 ° C in 5% CO_2 for 24 h. The media was then replaced with fresh media and the cells were treated with various concentrations of BLa, BILa, and BDILa (0, 0.25, 0.5, 1.0 and 2.0 μM) at 37 ° C in 5% CO_2 for 2 h under dark conditions. Then, the media in all plates were changed to a phenol-red free RPMI 1640 media and the cells were irradiated with a green light-emitting diode (LED), which had a wavelength of 530 nm (80%, 20 min), as previously described [42,43]. The irradiation power of the LED was approximately 9 mW. The cells were then incubated for further 24 h post-irradiation with the LED, and the viable cells were measured using a CellTiter 96® AQueous One Solution Cell Proliferation Assay according to the manufacturer's instruction.

2.2.9. Cellular Uptake by Flow Cytometry

To investigate the cellular uptake of the samples by HeLa, MCF-7

and Huh7 cells, flow cytometry was performed. Briefly, each cell line was seeded at 1 × 10^5 cells/well in a 6-well plate and incubated at 37 ° C in 5% CO_2 for 24 h. The incubated cells were then treated with the test samples (2.0 μM). After 2 h, the cells were collected and analyzed using an FC500 flow cytometer (Beckman coulter, CA, USA).

2.2.10. Theoretical Calculations

The molecular structures of the BODIPY derivatives were optimized using density functional theory (DFT), CAM-B3LYP function and 6-31G(d,p) basis set (LanL2DZ basis for I atoms) in a stepwise manner, and then the electronic states of the BODIPY derivatives were calculated using time-dependent DFT (TD-DFT) with the CAM-B3LYP function and 6-31G(d,p) basis set (LanL2DZ basis for I atoms), adding the water solvent environment, on a supercomputer to obtain information regarding excited states.

2.2.11. Statistical Analysis

All data were expressed as the mean ± standard deviation and compared by one-way analysis of variance (ANOVA), followed by the Tukey's multiple comparison test, using a Prism GraphPad 6 software (San Diego, CA, USA). A p value of < 0.05 was considered statistically significant in all analyses.

2.3. Results and Discussion

2.3.1. Synthesis and Design of Water-Soluble BODIPY Dyes

A three-step synthetic approach of the water-soluble and tumor-targeting BODIPY dyes is indicated in Scheme 2.1. The BODIPY core was synthesized via acid-catalyzed condensation reaction between dimethyl pyrrole and an acid chloride derivative, 5-bromovaleryl chloride, initially forming an unstable dipyrromethene hydrochloride salt intermediate. This intermediate subsequently rapidly reacts with the nearby boron trifluoride diethyl etherate in the presence of a base such as triethylamine, eventually affording the BODIPY core. Then, the conversion of the alkyl halide group of BODIPY into its alkyl azide analouge (BODIPY dye 1) was performed by treating the precursor dye with excess sodium azide (NaN_3). The second step entails the attachment of iodine atoms onto either the 2- or 2,6-position of the BODIPY core, employing *N*-iodosuccinimide (NIS) as the source of iodine atoms. It has been well known that the introduction of such heavy atoms onto BODIPY and aza-BODIPY dyes remarkably increases the intersystem crossing efficiency and consequently enhances generation of the singlet oxygen through an increase in spin-orbit coupling [11,15]. BODIPY dyes 2a and 2b were obtained in high yields (78% and 85%, respectively) by modifying the corresponding amounts of NIS and the reaction duration. The last step involves the incorporation of the lactose group through the straightforward CuAAC click reaction. The conjugation of the lactose moiety ultimately produced three lactose-modified BODIPY-based photosensitizers with inherently photodynamic therapeutic and tumor-targeting capabilities: BLa, BILa, and BDILa.

Scheme 2.1. Synthesis of the water-soluble and tumor-targeting, lactose-functionalized 4,4-difluoro-4-bora-3a,4a-diaza-s-indacene (BODIPY) dyes.

Crucial to our synthetic approach for the development of the BODIPY-based photosensitizers was the design of a facile, simple, and economic route that would deliver high reaction yields, reproducible, and can be performed without using elaborate experimental protocols. Hence, we used the CuAAC click reaction, which has been substantially employed for the production of a wide variety of functional carbohydrate-modified BODIPY derivatives due to its selectivity, versatility, and efficiency [34]. Herein, the CuAAC click reaction was performed under mild reaction conditions, has provided high yields and entailed an easy purification techniques. The three final BODIPY derivatives BLa, BILa, and BDILa were obtained via an easy recrystallization step in a methanol/ether solvent system and afforded in good yields (47% to 63%). Furthermore, the incorporation of the lactose group has resulted to an enhanced water-solubility of the resulting BODIPY dyes. The dyes BLa and BILa were totally dissolved in water, while BDILa could be readily dissolved in water by dilution from a stock solution in dimethyl sulfoxide (DMSO). Herein, we have prepared the sample stock solutions (100 μM) containing 0.5% (*v*/*v*) DMSO, as commonly practiced in biology related experiments [44]. In addition, ^{1}H-NMR spectroscopic characterizations were carried out to confirm the

structures of the synthesized BODIPY derivatives and additional ^{13}C-NMR spectroscopic analyses were done for the last three BODIPY dyes, BLa, BILa, and BDILa.

2.3.2. Theoretical and Photophysical Characterizations of Water-Soluble BODIPY Dyes

The photophysical characteristics of the synthesized water-soluble BODIPY-based derivatives BLa, BILa, and BDILa were assessed by measuring the samples' UV/Vis absorption and fluorescence in aqueous solution containing 0.5% (*v*/*v*) DMSO. The recorded emission and absorbance spectra of the synthesized BODIPY derivatives are depicted in Figure 2.1 and key values are listed in Table 2.1. All of the prepared BODIPY dyes demonstrated spectral properties unique to the BODIPY fluorophore. Intense absorbance peaks were positioned at 498, 510, and 526 nm for BLa, BILa, and BDILa, respectively, which can be attributed to the characteristic strong $S_0 \rightarrow S_1$ ($\pi \rightarrow \pi^*$) transition of the boradiazaindacene chromophore [45,46]. Moreover, at approximately 378 nm, a weaker and broad absorption band was observed, corresponding to the out-of-plane vibrations of the aromatic skeleton $S_0 \rightarrow S_2$ ($\pi \rightarrow \pi^*$) transition [47,48]. Although the absorption maxima of the BODIPY dyes were in the range of 498-526 nm, they were considered acceptable for the planned biological investigations. In addition, the emission spectra of the prepared BODIPY-based PS agents demonstrated approximate mirror images of their absorption spectra, signifying that the absorbing and emitting species have closely resembled corresponding structures. Furthermore, a distinguishable red-shift was observed in the absorption and emission spectra (12-28 nm and 14-32 nm,

respectively) of the resulting BODIPY dyes after the attachment of halogen atoms onto the BODIPY core. This is attributed to the heavy atom effect stemming from the attached halogen atom [15]. Moreover, the unhalogenated BODIPY dye BLa exhibited an emission peak positioned at approximately 510 nm and showed a high fluorescence quantum yield (~0.64). The subsequent iodination reaction resulted in a notable reduction in their respective fluorescence quantum yields (0.06 and 0.02 for BILa and BDILa, respectively) and a red-shift of the emission maxima (524 and 542 nm, respectively), relative to the uniodinated BLa. Such a decline in fluorescence quantum yields, as strongly affected by the heavy atom effect, indicates better photosensitizing properties in the iodinated BODIPY derivatives BILa and BDILa when compared to that of non-iodinated BLa.

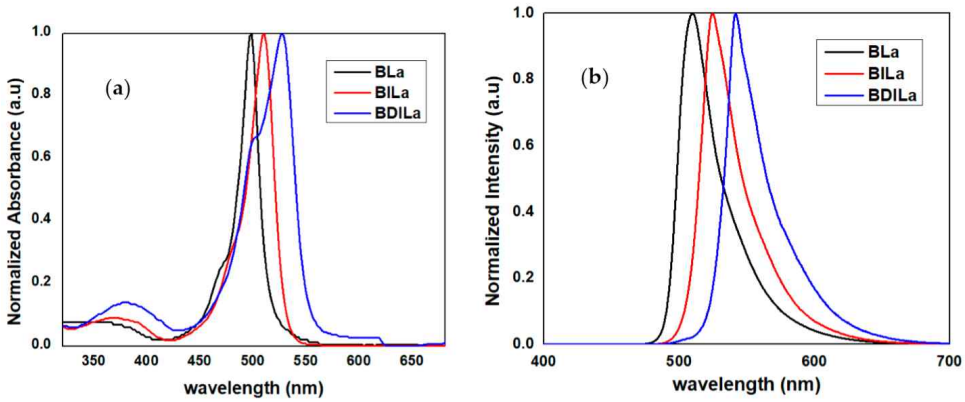

Figure 2.1. (**a**) absorption and (**b**) emission spectra of the water-soluble BODIPY dyes BLa, BILa, and BDILa in aqueous solution. Solutions were excited at their corresponding absorption maxima.

To additionally explain the electronic effects of iodination on the BODIPY's optical properties, theoretical analysis of the dyes' frontier molecular orbitals (MOs) were performed based on the optimized

Table 2.1. Optical parameters of the dyes BLa, BILa and BDILa.

	BLa	BILa	BDILa
λ_{ab} (nm)[a]	498	510	526
λ_{em} (nm)[a]	510	524	542
ΦF[b]	0.64	0.06	0.02
Φ_{Δ}[c]	0.01	0.27	0.47
ε (M^{-1} cm^{-1})	56,000	51,600	41,800

[a]in aqueous solution; [b]in methanolic solution; [c]in ethanolic solution.

molecular structures of the BODIPY dyes. As demonstrated in Table 2.2 and Figure 2.2, the destabilization of the HOMO caused by the substituted iodine atoms played a critical role in the narrowing the gap between highest occupied molecular orbital (HOMO) and lowest unoccupied molecular orbital (LUMO). Such destabilization resulted also in the increase of the oscillator strength and a red-shifted absorption band. Furthermore, a simulation of the BLa, BILa, and BDILa in water solution was performed. As shown in Figure 2.3, a blue-shift was observed in the calculated absorption spectra in the water solvent for the three compounds relative to that of the experimental values. Such shifts were also found to some reported BODIPY systems [48].

Table 2.2. Selected transition energies and wave function of Bla, BILa, and BDILa in the water solution.

	Excited State	Energy [eV]	λ [nm]	f[a]
BLa[b]	S1	2.995	414	0.63
BILa[c]	S1	2.959	419	0.70
BDILa[c]	S1	2.890	429	0.79

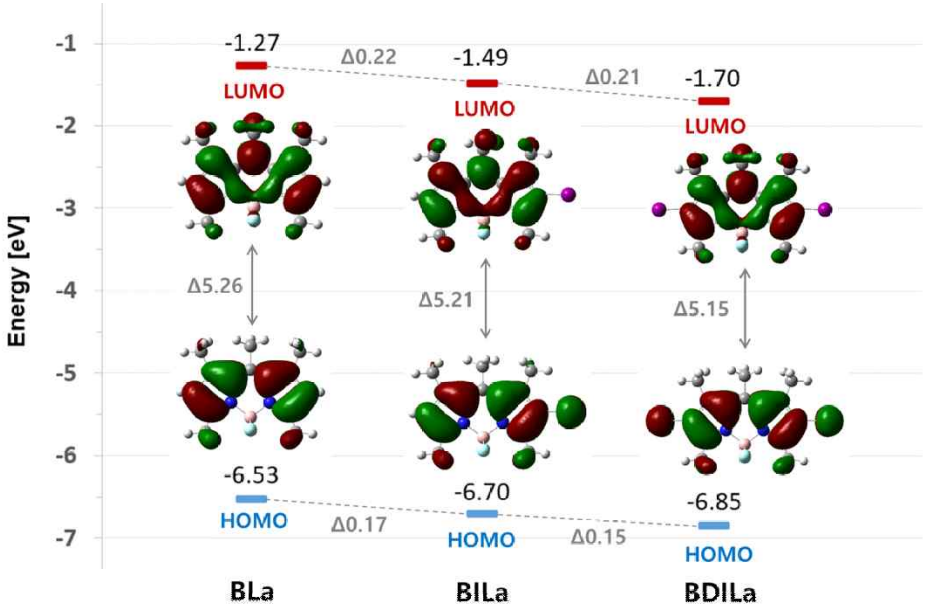

Figure 2.2. Highest occupied molecular orbital-lowest unoccupied molecular orbital (HOMO-LUMO) transition energies and wave function of BLa, BILa, and BDILa calculated using the density functional theory (DFT) method with the CAM-B3LYP functional and 6-31G(d,p) basis set (LanL2DZ basis for I atoms).

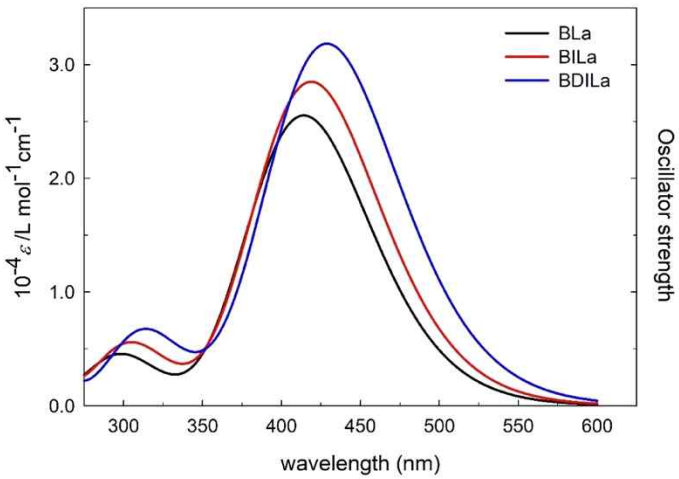

Figure 2.3. The simulated UV-Vis spectrum of BLa, BILa, and BDILa in water solution.

2.3.3. Singlet Oxygen Generation of Water-Soluble BODIPY Dyes

While an important factor for assessing the success of a PDT agent is its capacity to generate $^1O_2$ after a transfer of energy from the photosensitizer triplet excited state (T_1) to the surrounding molecular oxygen, the bulk of BODIPY-based photosensitizers have low singlet oxygen quantum yields since an intersystem crossing from a singlet to a triplet excited state is spin-forbidden. The absorbed energy is mostly contained in singlet excited states (S_n) and released as fluorescence for most compounds [49]. It generally required a spin-orbit perturbation for an effective intramolecular electronic transition between states of different spin multiplicities to take place [50]. Several reports have indicated that incorporating heavy atoms such as halogens directly onto the molecule, or confining the molecule within a heavy-atom-rich environment could result in significantly enhanced spin-orbit perturbations. These increased perturbations then influence the rates of the spin-forbidden intersystem crossing and facilitate the production of singlet oxygen [51,52]. Hence, the 2- and 2,6-positions of the BODIPY core were respectively conjugated with iodine atoms and their $^1O_2$ production capabilities were compared to that of the uniodinated BODIPY, which is heavily reliant solely on its intrinsic spin-orbit coupling capability in this process. Herein, an indirect detection of singlet oxygen was carried out to assess the $^1O_2$ generation efficiency of the synthesized BODIPY dyes via the photodegradation of a quencher, 1,3-diphenylisobenzofuran (DPBF). The DPBF rapidly reacts with $^1O_2$ to form an endoperoxide via a [4 + 2] cycloaddition reaction. The endoperoxide subsequently degrades to 1,2-dibenzoylbenzene, leading to the total loss of the conjugated π

-electron system and its unique absorption properties [53]. The photodegradation rates of the DPBF were monitored spectroscopically by observing the decrease in the quencher's absorption peaks at 424 nm [41].

Entrapment experiments were carried out by treating DPBF (50 μM) with the BODIPY-based PS agents (0-2.0 μM) in an air-saturated EtOH medium and subsequently irradiating the resulting solutions with a LED (λ_{max} = 500 nm, 9 mW/cm^2) light source. As indicated in Figure 2.4, the DPBF suffered an extensive photobleaching following treatment with the halogenated BODIPY dyes and LED irradiation. DPBF bleaching was exhibited as the marked absorbance peak in the region of 424 nm disappeared. As demonstrated in Fig. 2.4a, the incubation of DPBF with monoiodinated dye BILa led to a complete disappearance of the absorbance band after 10 min of LED irradiation, while the treatment with its diiodinated counterpart, BDILa, resulted in a more abrupt vanishing of the absorbance peak (~6 min, Fig. 2.4b).

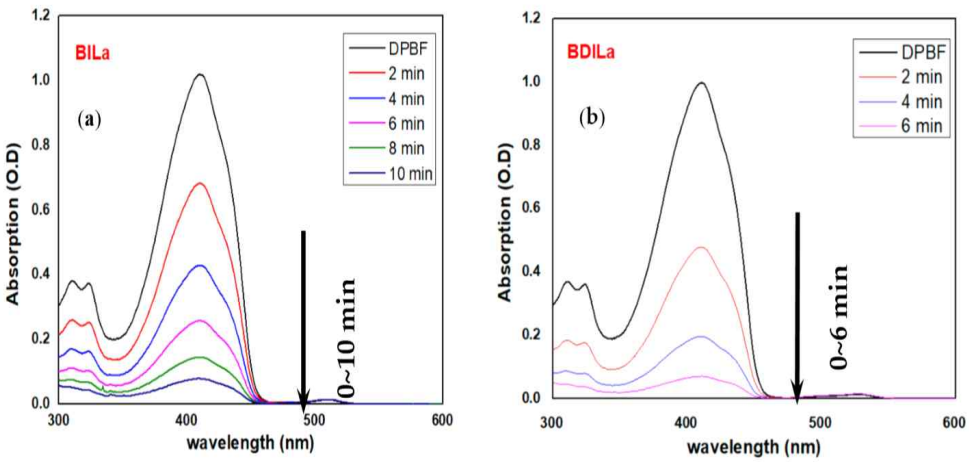

Figure 2.4. Time-dependent absorption spectra of 1,3-diphenylisobenzofuran (DPBF) in EtOH with **(a)** BILa and **(b)** BDILa after LED light excitation at 500 nm.

In contrast, no notable photodegradation of DPBF was observed for the uniodinated control, as the unique DPBF absorbance band at around 424 nm was visible even after 70 min of uninterrupted exposure to the light source. The $^1O_2$ quantum yields (Φ_Δ) of the prepared BODIPY dyes were also quantified employing a reference standard, hematoporphyrin (HP), whose Φ_Δ is known (0.53 in EtOH). The decay curves of the absorption density for DPBF in the presence of the test samples and HP were linearly fitted and presented in Figures 2.5. The halogenated BODIPY dyes, BILa and BDILa, incurred $^1O_2$ quantum yields of 0.27 and 0.47, respectively, while the uniodinated control could not produce $^1O_2$ under the same experimental conditions (Φ_Δ = 0.01). These outcomes collectively show that the iodination reaction of the BODIPY core achieved the elevated generation of singlet oxygen following LED illumination. In the case of BDILa, the additional heavy iodine atom prompted additional spin-orbit perturbations, resulting in its superior capacity to produce $^1O_2$, as demonstrated by the abrupt photodegradation rate of DPBF and the higher calculated $^1O_2$ quantum yield, relative to the monoiodinated derivative BILa.

2.3.4. Cytotoxicity Assessment of the Water-Soluble BODIPY Dyes

Another significant consideration when assessing the photosensitizer's potential as a PDT agent is their capability to induce minimal cytotoxicity in the dark, but excellent toxicity following irradiation with light. Herein, the cytotoxicities of the prepared BODIPY dyes were investigated against three distinct malignant cell lines (MCF-7, HeLa, and Huh7). The assessments of vell viability

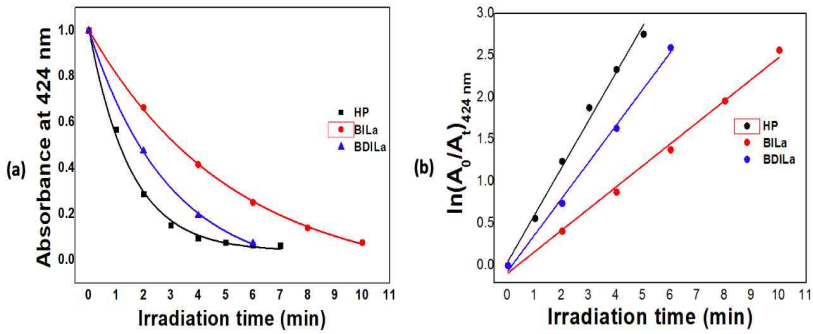

Figure 2.5. (a) Normalized decay curves of the absorption density at λ_{ex}=424 nm for the DPBF in the presence of the **BILa** and **BDILa** against HP (normalized by the absorbance intensity at t=0 min). (b) linearly fitted degradation rates for the DPBF in the presence of the test samples and HP.

were carried out employing the [3-(4,5-dimethylthiazol-2-yl)-5-(3-carboxymethoxyphenyl)-2-(4-sulfophenyl)-2H-tetrazolium] (MTS) assay. In any metabolically active cell, the MTS, a mitochondrial succinate dehydrogenase substrate (SDH, EC 1.3.5.1), is readily converted to formazan by the dehydrogenase enzymes. The formazan generated by the enzymes is directly correlated to the culture's number of living cells and can be monitored spectroscopically at 490 nm [54]. Initially, the three cancer cell lines were treated with the synthesized BODIPY-based PS agents of various concentrations and the amount of viable cells were determined in the absence and presence of 530 nm LED light illumination. To account for the absorbance of the MTS tracker (background), their absorbance values were subtracted from those of the solutions containing the treated and control cells. As demonstrated in Figure 2.6, negligible toxicities in the dark of all the prepared BODIPY dyes were found against Huh7, and the cells were found to be least 96% viable, even after treatment with a maximum dye concentration (2.0 μ

M). The other two cancer cell lines, HeLa and MCF-7, have manifested the same low cytotoxicities in the dark (Figures 2.7, 2.8, respectively), wherein all three BODIPY-based PS agents demonstrated 96% cell viability or above, even after incubation at a maximum concentration (2.0 μM). The low toxicities showed by the synthesized BODIPY dyes in the absence of light irradiation are a possible manifestation of their advantageous biocompatibility, stemming from the biological prevalence of the conjugated lactose group.

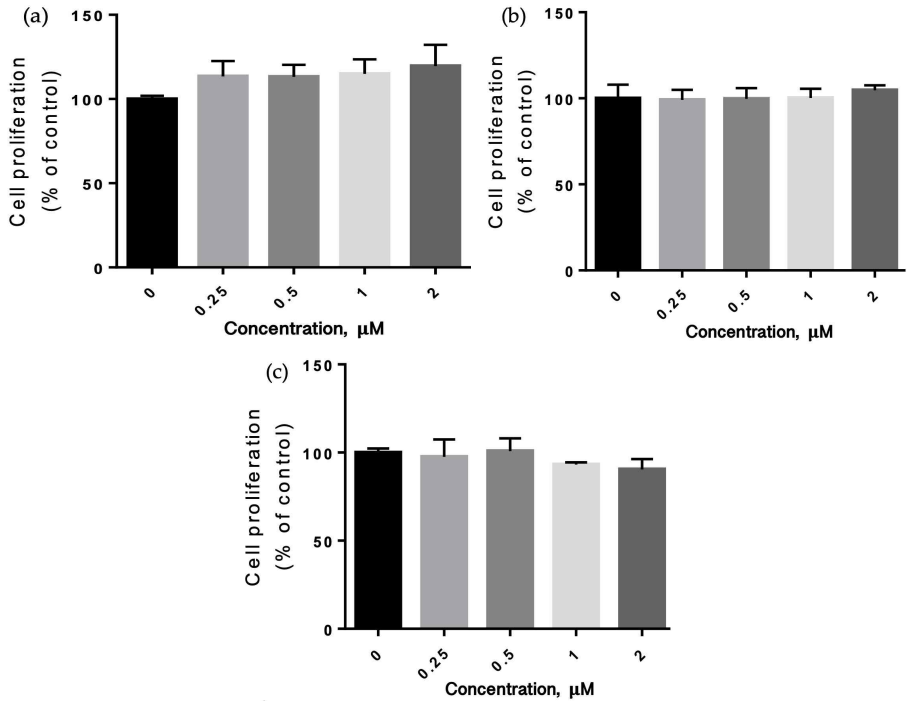

Figure 2.6. Cell viabilities of Huh7 cells after incubated with (a) BLa, (b) BILa, and (c) BDILa under dark conditions.

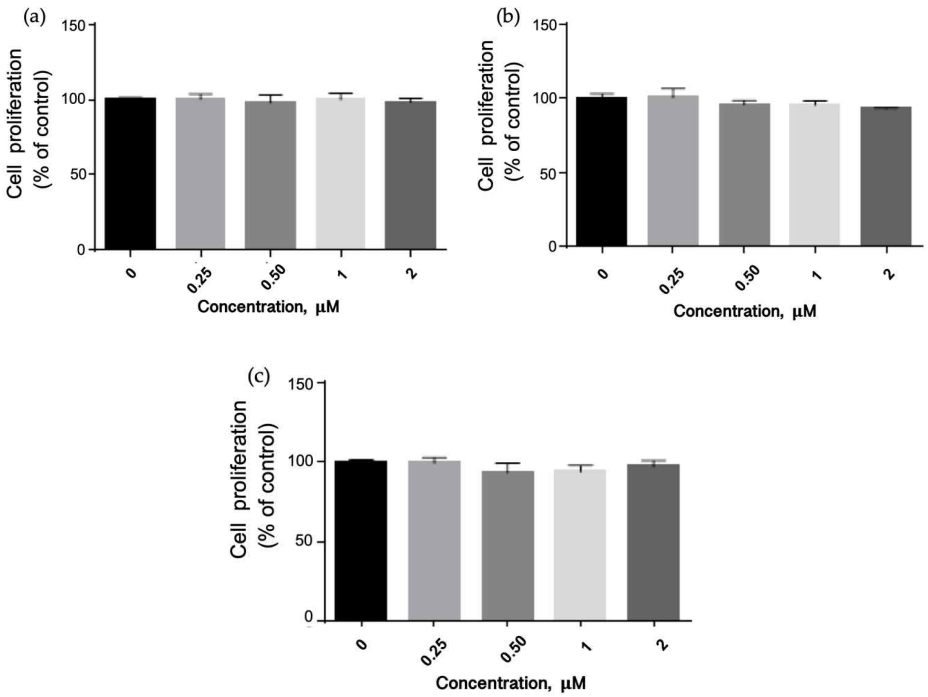

Figure 2.7 Cell viabilities of HeLa cells after incubated with (a) BLa, (b) BILa, and (c) BDILa under dark conditions.

2.3.5. Cellular Uptake by Flow Cytometry

There has been a great association between the photosensitizer efficacy and effective cellular uptake [55,56]. Hence, a quantitative investigation of the cellular uptake of the synthesized BODIPY derivatives in Huh7, MCF-7, and HeLa cells was performed using flow cytometry. The cells were treated with the synthesized BODIPY dyes (2.0 μM) at 37 °C for 2h and subsequently subjected to fluorescence-activated cell sorting (FACS) analysis. The untreated cell

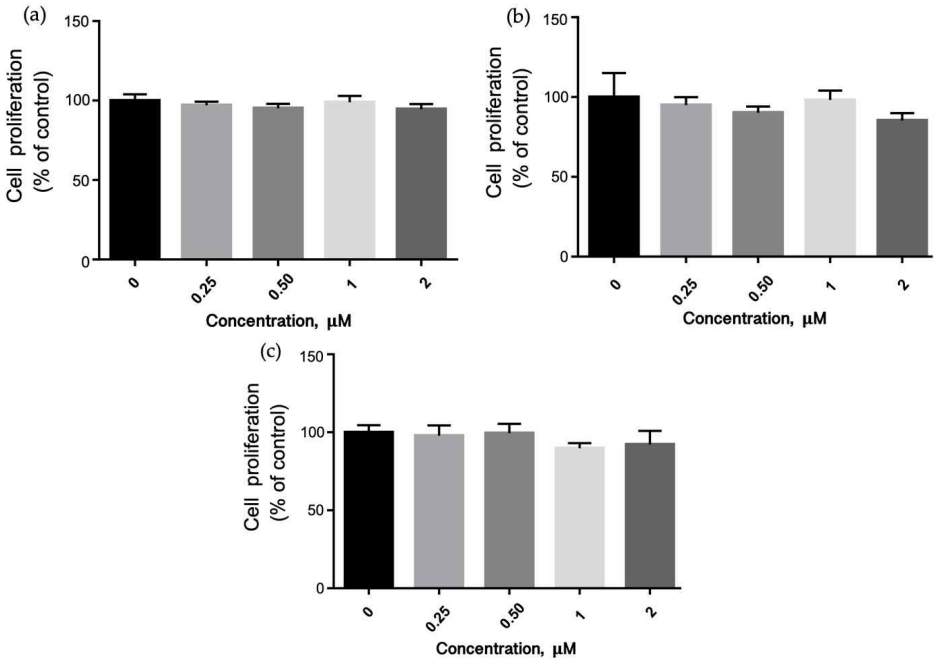

Figure 2.7. Cell survival rates of MCF-7 cells after treatment with (a) BLa, (b) BILa, and (c) BDILa under dark conditions.

lines, as a control setup, were also subjected to FACS under the exact experimental conditions. The corrected median fluorescence intensities (MFI) of the BODIPY dyes against the treated malignant cell lines were summarized in Table 2.3. As shown in Figure 2.9, the corresponding controls (without BODIPY dyes) in all three cancer cell lines demonstrated low fluorescence intensities attributable to their intrinsic mitochondrial autofluorescence. This signifies that the fluorescence intensities exhibited by the BODIPY-incubated cancer cell lines could be attributed to the intracellularly accumulated BODIPY dyes. The relative cellular internalization of the PS agents across all cell types was BDILa < BILa < BLa.

Table 2.3. Corrected median fluorescence intensities (MFI) of the dyes BLa, BILa and BDILa against treated cancer cell lines.

	BLa (log)[a]	BILa (log)[a]	BDILa (log)[a]
HeLa	7807 ± 460	5102 ± 123	2380 ± 100
Huh7	12083 ± 632	7589 ± 84	4138 ± 70
MCF-7	38952 ± 1730	5414 ± 447	2938 ± 219

[a]Data are mean ± SD (n = 3).

The cellular uptake for the halogenated BODIPY derivatives, BILa and BDILa when compared to their corresponding parent dye BLa, distinctly showed that the introduction of iodine atoms onto the BODIPY core resulted in the decrease of their capability to be internalized by the treated malignant cells. For instance, treatment of Huh7 cells with the control dye BLa showed the highest fluorescence intensity (Figure 5), suggesting an effective cellular localization of the incorporated dye. The mean fluorescence for Huh7 cells incubated with control dye BLa was approximately 18-fold higher relative to that of the untreated cells, whereas the halogenated-BODIPY counterparts (BILa and BDILa) exhibited approximate increases of 12- and 7-fold, respectively. This observation was similar for the other two malignant cell lines (Table 3). Both MCF-7 and HeLa cells treated with BDILa, BILa, and BLa showed an enhanced mean fluorescence intensities of approximately ~5-, ~9 to 11, and ~16-fold, respectively, when compared to that of the untreated cells. The collective cellular uptake profiles of the BODIPY dyes corroborate with the notion that molecular synthetic modifications can lead to significant variations in partition coefficient values. It is worth noting that the overall hydrophilicity/lipophilicity of the dye plays a crucial part in photosensitizer-cell surface interactions [57]. Consequently, a right balance between the dye's lipophilicity and hydrophilicity is imperative to attain sufficient cellular uptake and biodistribution. Unrestricted lipophilicity would block the dye's transport through the blood vessels, while excessive hydrophilicity

would empede its penetration into cell membranes [35]. Although the added iodine atoms aid the effective production of $^1O_2$, they however reduced the overall hydrophilicity of the molecules, leading to decreased cellular uptake of the BODIPY dyes. In particular, BDILa showed relatively low cellular uptake, as demonstrated by its lower fluorescence intensity, when compared to that of BILa and BLa. In spite of the slight decrease in cellular uptake, both of the halogenated BODIPY dyes brought about excellent phototoxicity towards the tested malignant cell lines, thus suggesting that the observed cellular uptake is adequate for photodynamic therapy.

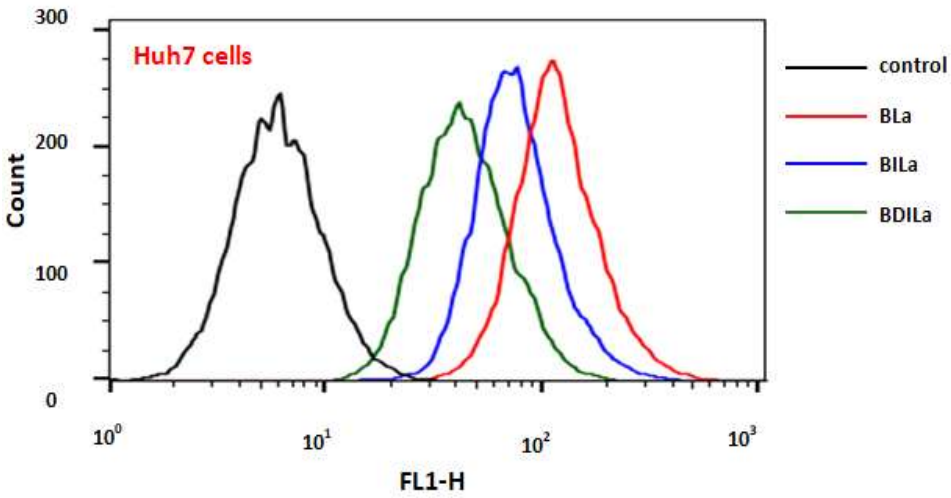

Figure 2.9. The cellular uptake of the BODIPY dyes BLa, BILa, and BDILa in Huh7 cells via fluorescence-activated cell sorting (FACS) analysis.

It is also worth noting that tumor cell surfaces and membranes have numerous overly expressed proteins, transporter molecules, and receptors. Such overly expressed transporters and receptors are unique and specific for a particular cell line. For instance, liver cancer cells Huh7 are well known to possess overexpressed asialoglycoproteins

(ASGPR) and C-lectin type receptors [58,59], while human breast cancer cells MCF-7 have cell surfaces rich in mannose-receptors [18]. Thus, targeting of these overly expressed receptors can be beneficial as they can interact with the targeting moieties through carbohydrate-mediated cell recognition processes [24,25]. Hence, to assess the tumor-targeting capacities of the synthesized BODIPY dyes, the cellular uptake profiles among all the treated malignant cell lines were compared. The conjugated lactose group of the prepared BODIPY-based PSs works as the targeting moiety that can selectively interact with a specific overexpressed receptor on the surfaces of the tumor cells. The results showed that the transfection of the lactose-functionalized BODIPY dyes were found highest in Huh7 cell, compared to that of the other two malignant cell lines. As mentioned, the surfaces and membranes of Huh7 cells have an abundance of overexpressed ASGPR and C-lectin type receptors, which have been well known to selectively bind to the galactose and galactose-modified macromolecules [60,61]. This may account for the incurred higher transfection of the BODIPY dyes in Huh7 cells, via enhanced carbohydrate-protein interactions, demonstrating the remarkable tumor-targeting capability of the water-soluble lactose-functionalized BODIPY dyes.

2.3.6. Photodynamic Anticancer Activity of the Water-Soluble BODIPY Dyes

The photodynamic therapeutic capability of prepared BODIPY dyes is reliant on their effectiveness in generating ROS, particularly singlet oxygen, following light irradiation [62,63]. Thus, we next investigated the toxicity of the synthesized BODIPY-based PSs BLa, BILa, and BDILa after irradiation with LED light (530 nm) for approximately 20 min. The

halogenated BODIPY dyes brought about significant cytotoxic effects ($p < 0.05$) in a dose-dependent manner in all three cancer cell lines. In the case of HeLa cells (Figure 2.10a,d), both BILa and BDILa induced cytotoxic effects even at the lowest used concentration (0.25 μM), and the severity of toxicity increased with their increasing concentration. The viability of HeLa cells dropped to below 10% and nearly 0%, following treatment with 1.0 μM and 2.0 μM of both dyes, respectively. The IC_{50} for BILa and BDILa against HeLa cells were calculated to be 0.53 μM and 0.55 μM, respectively. The MCF-7 cells sustained the same dose-dependent toxicities (Figure 2.10b,e), wherein BILa and BDILa showed evident toxic effects at a concentration of 0.5 μM and the induced cytotoxicities increased at higher concentrations. The calculated IC_{50} against MCF-7 cells was found to be 0.56 μM and 0.61 μM for BILa and BDILa, respectively.

As demonstrated in Figure 2.10c, the mono-iodinated BODIPY derivative BILa achieved significant cytotoxic effects ($p < 0.05$) to Huh7 cells at a concentration of 0.50 μM, while its diiodinated analogue BDILat induced significant toxic effects ($p < 0.05$) at a lower concentration of 0.25 μM (Figure 2.10f). Notably, BDILa showed 1.5-fold higher photo-killing efficacies, across all tested cancer cells, at concentrations above 0.5 μM when compared to that of the monoiodinated BILa. Furthermore, the calculated IC_{50} for BILa and BDILa against Huh7 cells were estimated to be 0.60 μM and 0.50 μM, respectively. The superior PDT capabilities of BDILa is highly expected, as the additional iodine atom allows enhanced generation of $^1O_2$ compared to its monoiodinated counterpart, leading to superior photodynamic therapeutic properties. These PDT effects are consistent with fluorescence and $^1O_2$ quantum yield results for the dyes, as shown in Table 1.1.

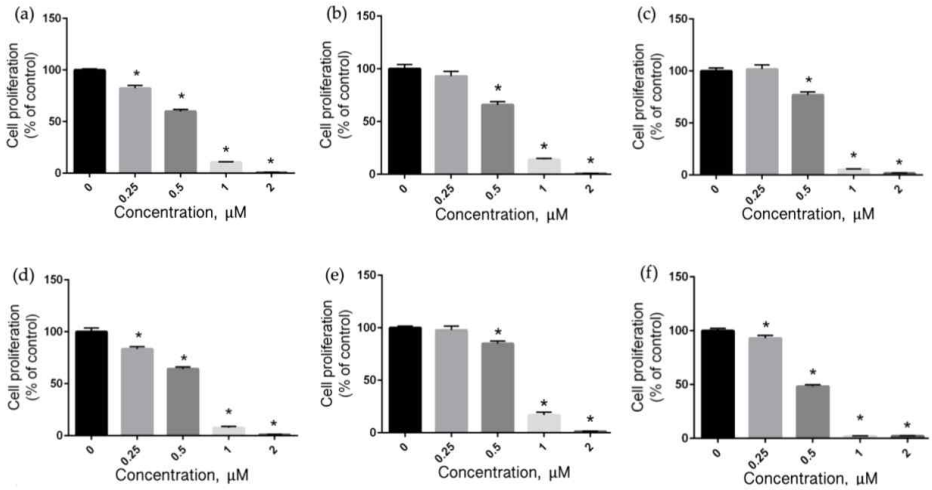

Figure 2.10. Dose-dependent cytotoxicities of synthesized BODIPYs. Cell survival rates of (**a**) HeLa, (**b**) MCF-7, and (**c**) Huh7 cells after treatment with BILa; (**d**) HeLa, (**e**) MCF-7, and (**f**) Huh7 cells after treatment with BDILa under LED light irradiation at 530 nm. *$p < 0.05$ compared to control (0 μM).

In contrast, the uniodinated control BLa showed no significant cytotoxicities against the tested cancer cells even after LED light exposure (Figure S8). This was evidenced in cell viabilities retained at 95% and above. There was also no significant change in the cell viabilities for both HeLa and Huh7 cells after incubation with BLa and subsequent LED light irradiation. While the MCF-7 cell viability has significant decreased ($p<0.05$) after treatment with BLa, the cell survival rates were still considered high (at least 80%) relative to that of the halogenated BODIPY dyes. Overall, these results indicated that the synthesized BODIPY-based PSs were biocompatible and non-toxic to cells in the dark, and induced cytotoxicity only upon LED light irradiation, attributable to the generation of reactive $^1O_2$. The PDT levels of the prepared BODIPY PS agents are quite comparable to other PS agents reported in the literature for PDT application, including porphyrin- and phtalocyanine-based photosensitizers [64-67].

2.4. Conclusions

Herein, the synthesis of water-soluble BODIPY PS agents conjugated with a lactose group was reported. The synthesized BODIPY derivatives were subjected to thorough photophysical and biological investigations as they were assessed as photosensitizers in photodynamic therapy. The introduction of iodine atoms onto the BODIPY core resulted in the efficient generation of $^1O_2$. Furthermore, the BODIPY dyes exhibited no cytotoxicities in the dark to the three tested tumor cell lines (MCF-7, Huh7, and HeLa). The halogenated BODIPY-based PS agents induced superior toxic effects against the tested cancer cell lines following irradiation with LED light, exhibiting their capabilities as potential photosensitizers for cancer treatment. The prepared BODIPY dyes demonstrated an effective cellular uptake by the tested cell lines, particularly by Huh7 cells. Such effective internalization of the cell lines is attributed to the carbohydrate-mediated recognition processes between the targeting biomolecule lactose, and specific receptors overexpressed oh the surfaces of the tumor cells. The collective results presented in this study signify an important contribution in the field of PDT, by providing a facile synthetic approach for producing water-soluble BODIPY dyes that are biocompatible, can target tumor cells, and photodynamic therapeutic capable.

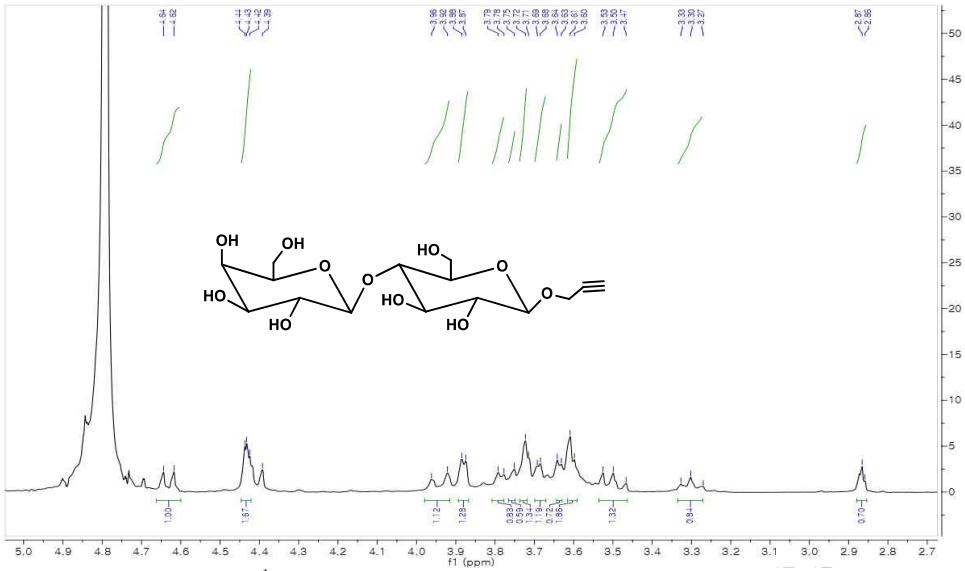

^{1}H-NMR spectrum of lactose-propargyl.

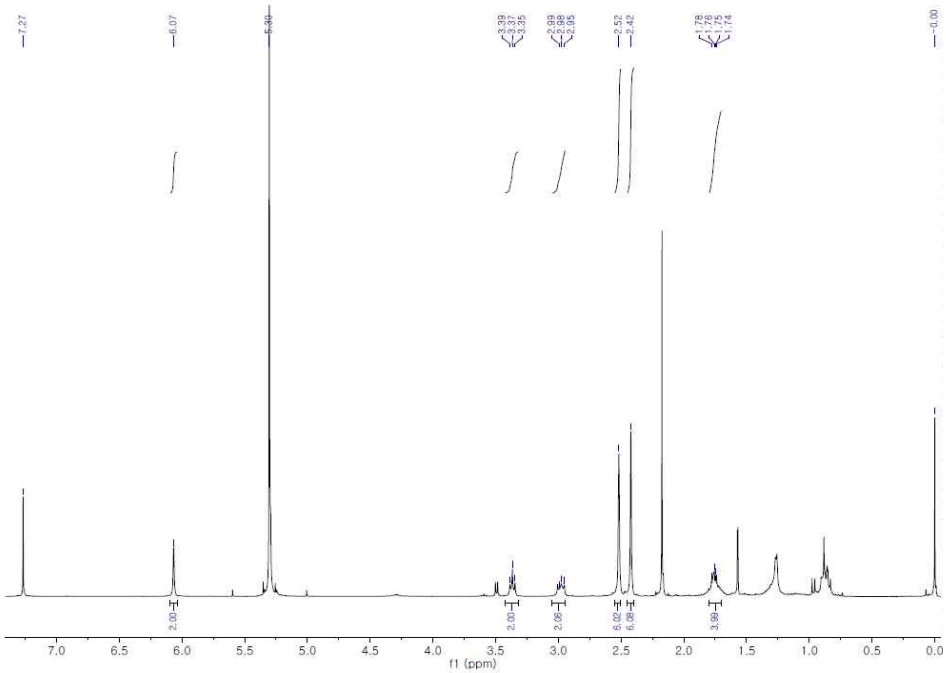

^{1}H-NMR spectrum of BODIPY dye 1.

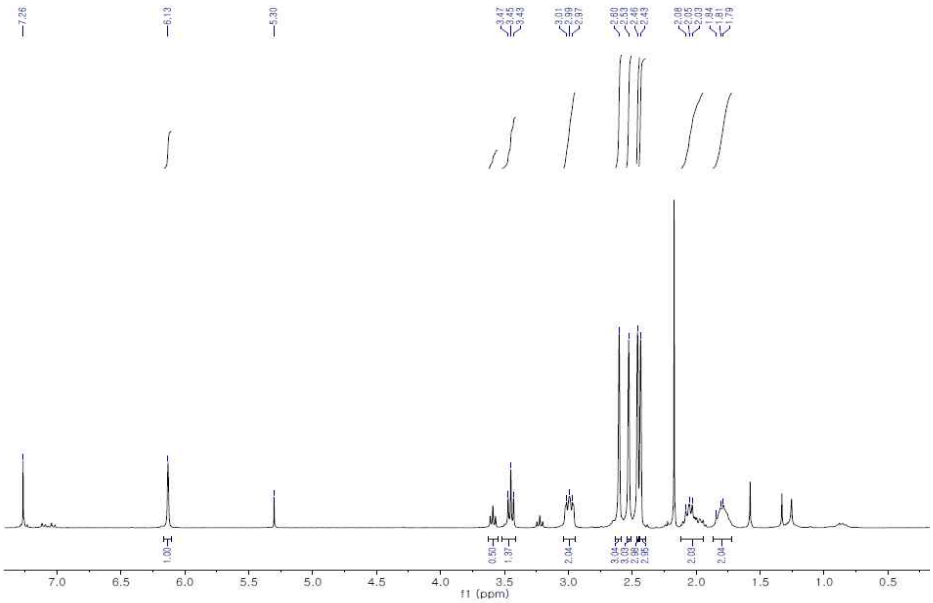

^{1}H-NMR spectrum of BODIPY derivative 2a.

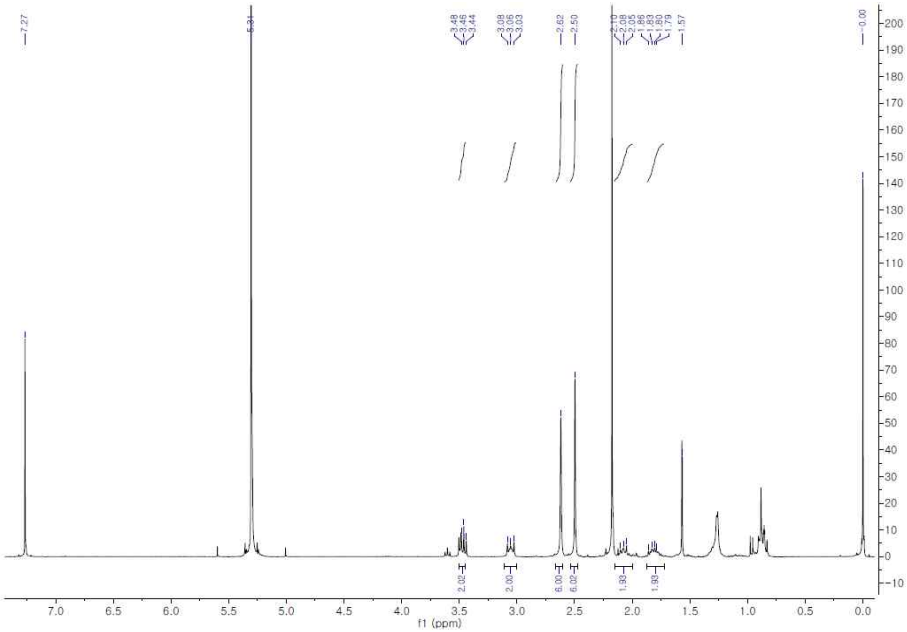

^{1}H-NMR spectrum of BODIPY derivative 2b.

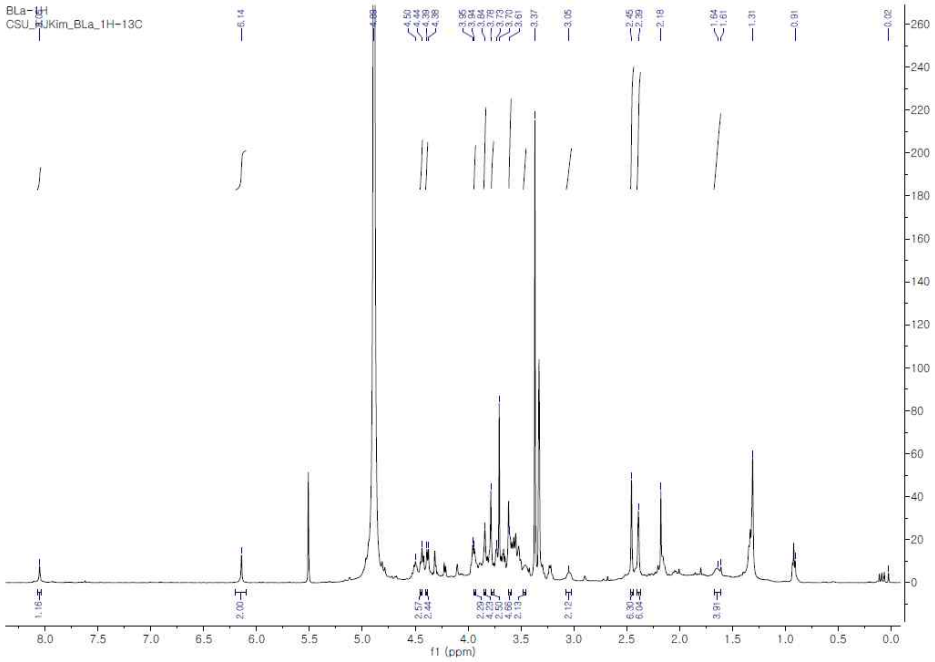

^{1}H-NMR spectrum of tumor-targeted water-soluble BODIPY BLa.

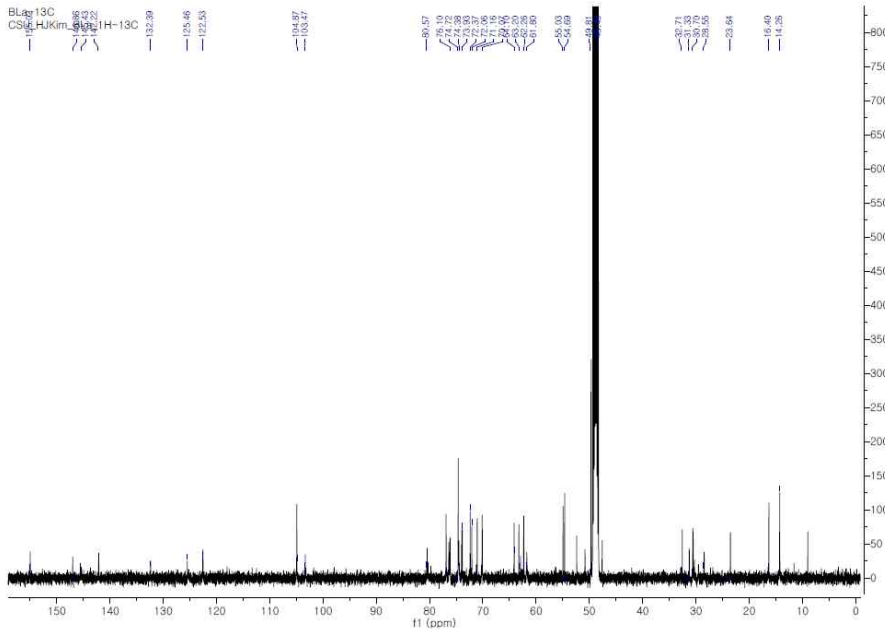

^{13}C-NMR spectrum of tumor-targeted water-soluble BODIPY BLa.

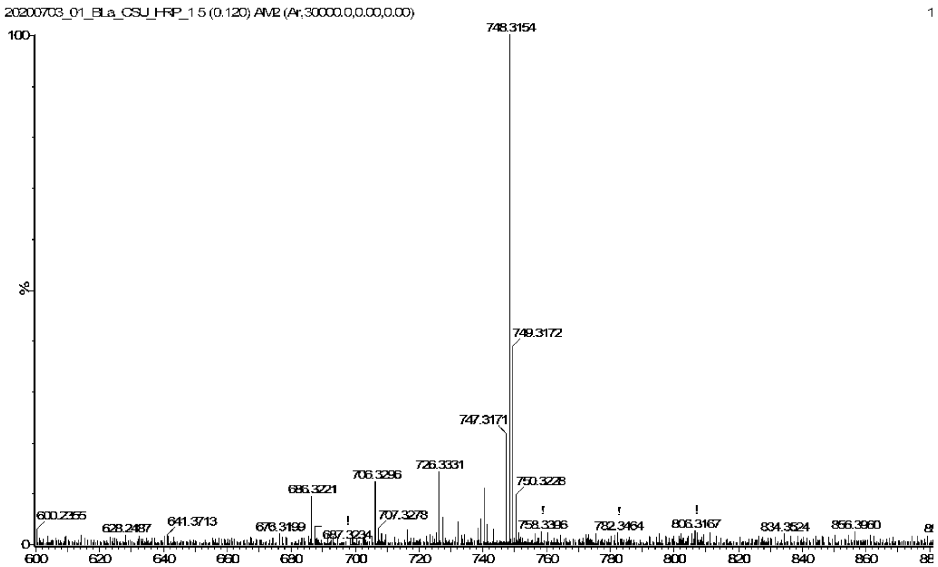

HR-ESI mass spectrum of tumor-targeted water-soluble BODIPY BLa.

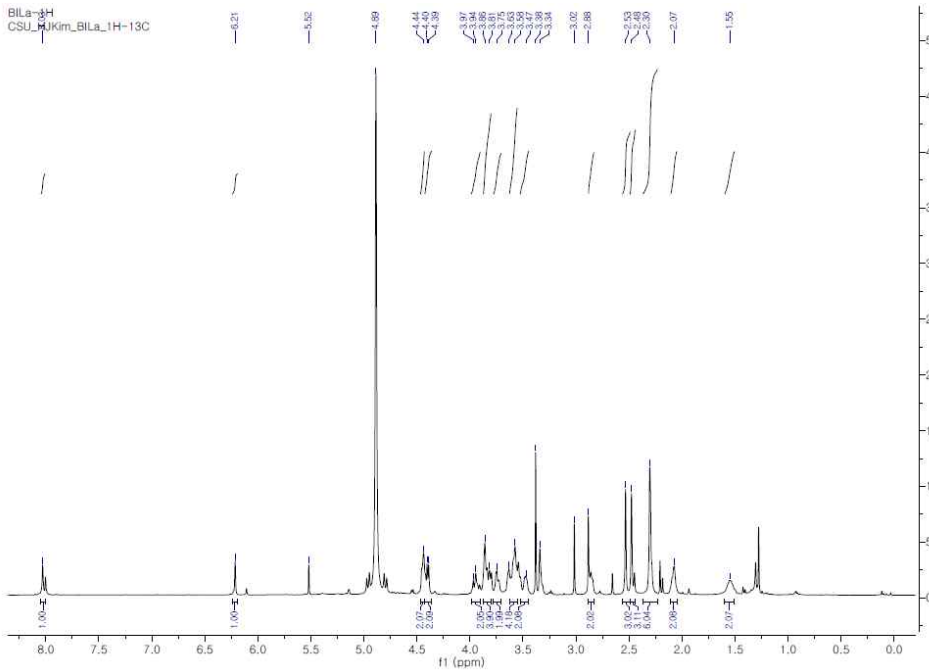

^{1}H-NMR spectrum of tumor-targeted water-soluble BODIPY BILa.

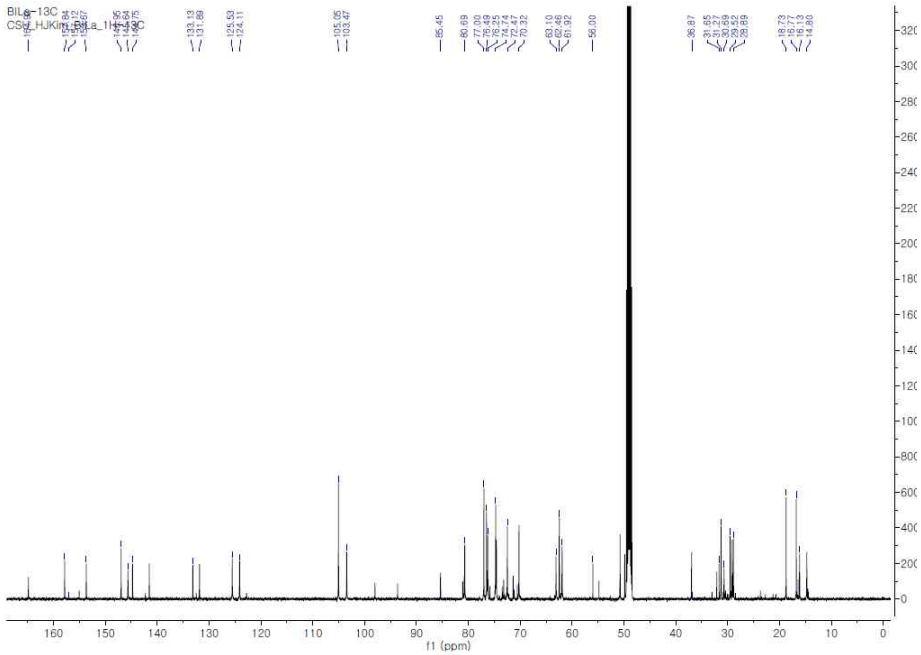

^{13}C-NMR spectrum of tumor-targeted water-soluble BODIPY BILa.

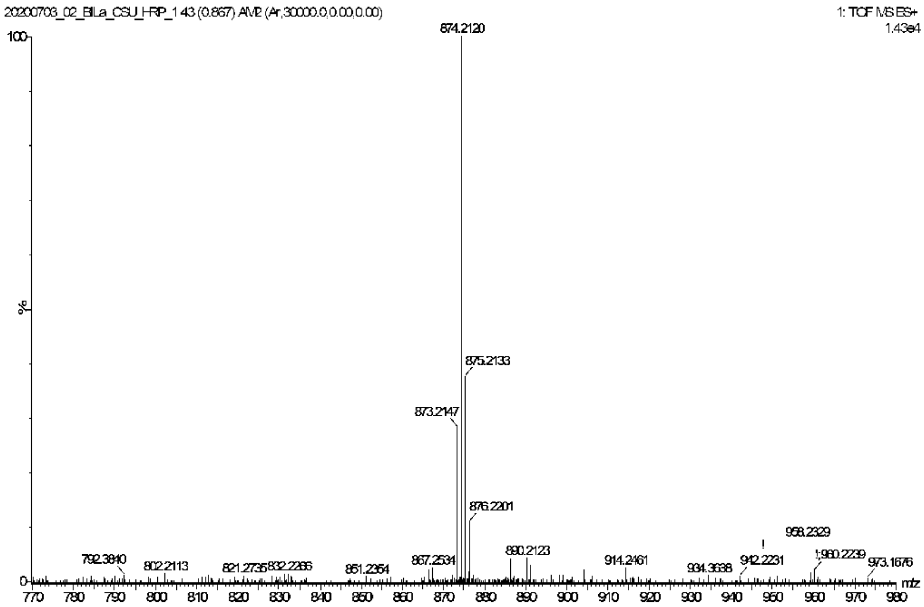

HR-ESI mass spectrum of tumor-targeted water-soluble BODIPY BILa.

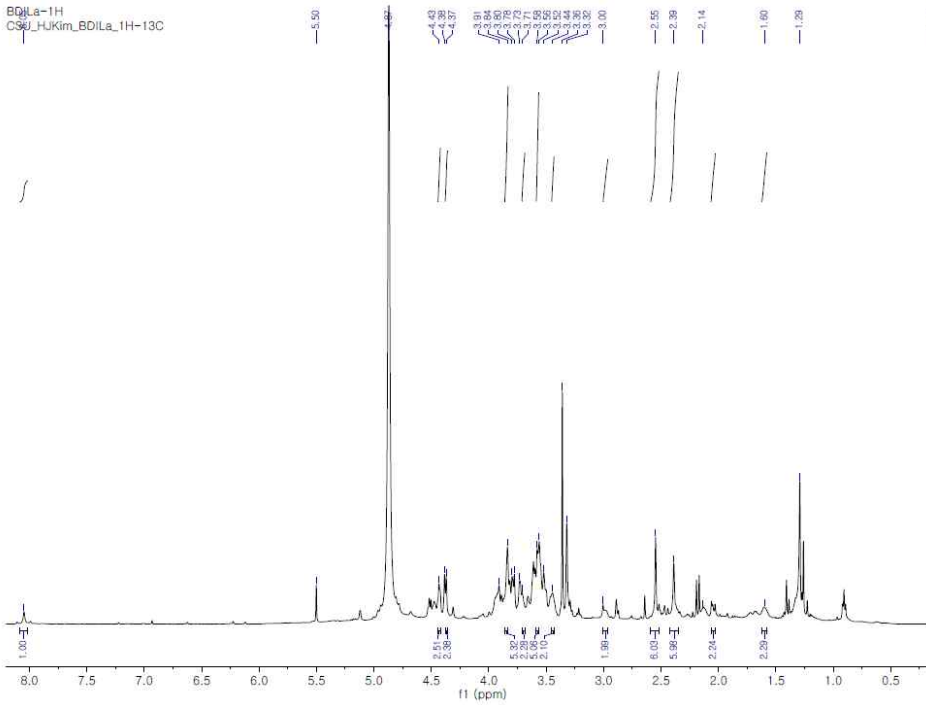

^{1}H-NMR spectrum of tumor-targeted water-soluble BODIPY BDILa.

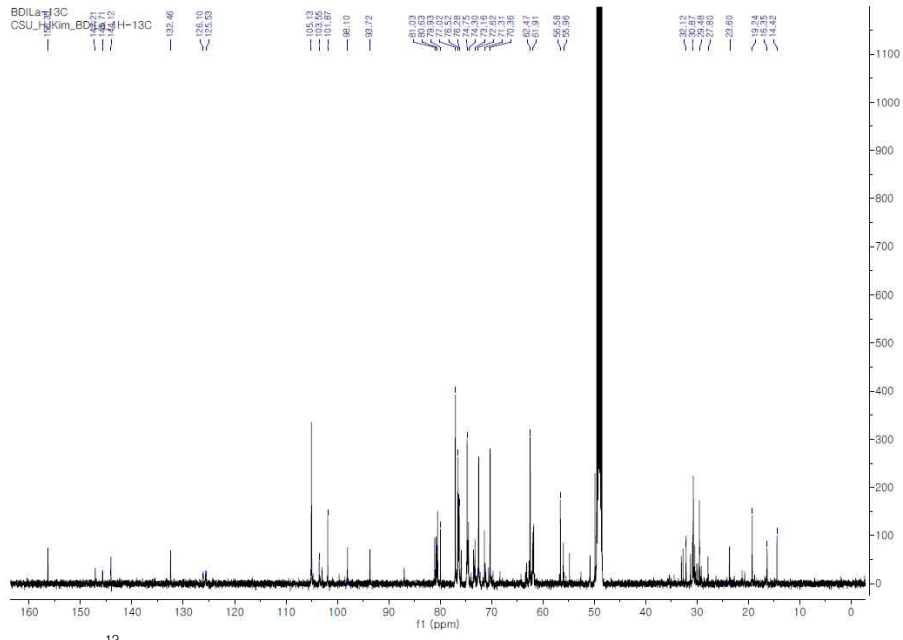

^{13}C-NMR spectrum of tumor-targeted water-soluble BODIPY BDILa.

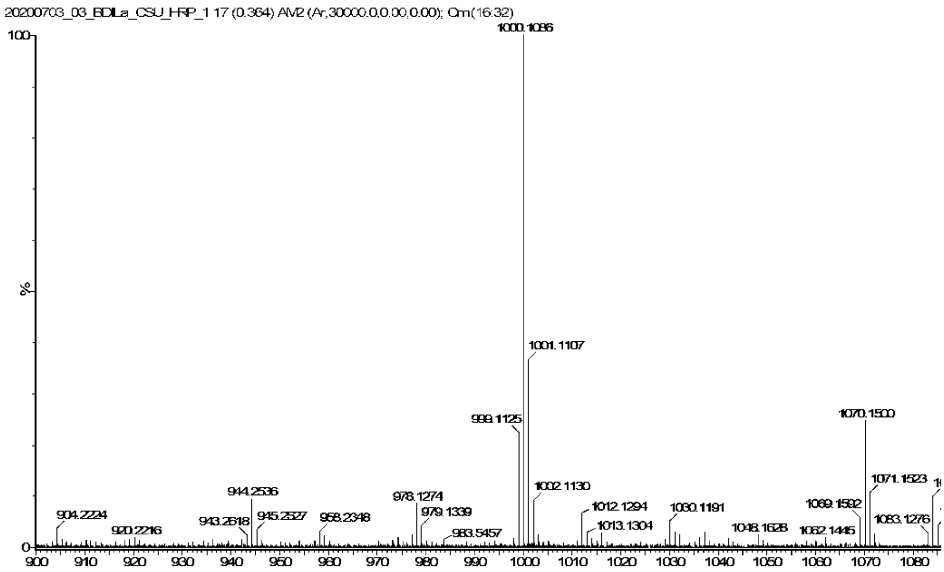

HR-ESI mass spectrum of tumor-targeted water-soluble BODIPY BDILa.

2.5. References

[1] Atilgan, S.; Ekmekci, Z.; Dogan, A.L.; Guc, D.; Akkaya, E.U. *Chem. Commun.* **2006**, *42*, 4398-4400.

[2] Kamkaew, A.; Lim, S.H.; Lee, H.B.; Kiew, L.V.; Chung, L.Y.; Burgess, K. *Chem. Soc. Rev.* **2013**, *42*, 77-88.

[3] Zhou, Y.; Cheung, Y.K.; Ma, C.; Zhao, S.; Gao, D.; Lo, P.C.; Fong, W.P.; Wong, K.S.; Ng, D.K. *J. Med. Chem.* **2018**, *61*, 3952-3961.

[4] Nyman, E.S.; Hynninen, P.H. *J. Photochem. Photobiol. B Biol.* **2004**, *73*, 1-28.

[5] Wainwright, M.; Phoenix, D.A.; Rice, L.; Burrow, S.M.; Waring, J. *J. Photochem. Photobiol. B Biol.* **1997**, *40*, 233-239.

[6] Zhang, W.; Li, G.; Lin, Y.; Wang, L.; Wu, *J. Biomater. Sci. Polym. Ed.* **2017**, *8*, 1935-1949.

[7] Lim, S.H.; Thivierge, C.; Nowak-Sliwinska, P.; Han, J.; Van Den Bergh, H.; Wagnieres, G.; Burgess, K.; Lee, H.B. *J. Med. Chem.* **2010**; *53*, 2865-2874.

[8] Lissi, E.A.; Encinas, M.V.; Lemp, E.; Rubio, M.A. *Chem. Rev.* **1993**, *93*, 699-723.

[9] Uzdensky, A.B.; Iani, V.; Ma, L.; Moan, J. *Photochem. Photobiol.* **2002**, *76*, 320-328.

[10] Robert Sjoback, J.N.; Kubista, M. *Spectrochim. Acta Part. A* **1995**, *51*, 7-21.

[11] Yogo, T.; Urano, Y.; Ishitsuka, Y.; Maniwa, F.; Nagano, T. *J. Am. Chem. Soc.* **2005**, *127*, 12162-12163.

[12] Verwilst, P.; David, C.C.; Leen, V.; Hofkens, J.; de Witte, P.A.M.; De Borggraeve, W.M. *Bioorg. Med. Chem. Lett.* **2013**, *23*, 3204-3207.

[13] Awuah, S.G.; Polreis, J.; Biradar, V.; You, Y. *Org. Lett.* **2011**, *13*, 3884-3887.

[14] Kowada, T.; Maeda, H.; Kikuchi, K. *Chem. Soc. Rev.* **2015**, *44*, 4953-4972.

[15] Gorman, A.; Killoran, J.; O'Shea, C.; Kenna, T.; Gallagher, W.M.; O'Shea, D.F. *J. Am. Chem. Soc.* **2004**, *126*, 10619-10631.

[16] Zhang, Q.; Cai, Y.; Li, Q.Y.; Hao, L.N.; Ma, Z.; Wang, X.J.; Yin, J. *Chem. Eur. J.* **2017**, *23*, 14307-14315.

[17] Li, Z.; Zheng, M.; Guan, X.; Xie, Z.; Huang, Y.; Jing, X. *Nanoscale* **2014**, *6*, 5662-5665.

[18] Zhang, Q.; Cai, Y.; Wang, X.J.; Xu, J.L.; Ye, Z.; Wang, S.; Seeberger, P.H.; Yin, J. *ACS Appl. Mater. Interfaces* **2016**, *8*, 33405-33411.

[19] Reddington, M.V. *Bioconjug. Chem.* **2007**, *18*, 2178-2190.

[20] Niu, S.L.; Ulrich, G.; Ziessel, R.; Kiss, A.; Renard, P.-Y.; Romieu, A. *Org. Lett.* **2009**, *11*, 2049-2052.

[21] Katritzky, A.R.; Cusido, J.; Narindoshvili, T. *Bioconjug. Chem.* **2008**, *19*, 1471-1475.

[22] Kang, B.; Opatz, T.; Landfester, K.; Wurm, F.R. *Chem. Soc. Rev.* **2015**, *44*, 8301-8325.

[23] He, X.-P.; Zeng, Y.-L.; Zang, Y.; Li, J.; Field, R.A.; Chen, G.-R. *Carbohydr. Res.* **2016**, *429*, 1-22.

[24] Zheng, X.; Pandey, R.K. P. *Anti-Cancer Agents Med. Chem. (Formerly Curr. Med. Chem. Agents)* **2008**, *8*, 241-268.

[25] Hao, E.; Jensen, T.J.; Vicente, M.G.H. *J. Porphyr. Phthalocyanines* **2009**, *13*, 51-59.

[26] Li, M.; Zhang, W.; Wang, B.; Gao, Y.; Song, Z.; Zheng, Q.C. *Int. J. Nanomedicine* **2016**, *11*, 5645.

[27] Liang, H.F.; Chen, C.T.; Chen, S.C.; Kulkarni, A.R.; Chiu, Y.L.; Chen, M.C.; Sung, H.W. *Biomaterials* **2006**, *27*, 2051-2059.

[28] Zheng, G.; Graham, A.; Shibata, M.; Missert, J.R.; Oseroff, A.R.; Dougherty, T.J.; Pandey, R.K. *J. Org. Chem.* **2001**, *66*, 8709-8716.

[29] Li, G.; Pandey, S.K.; Graham, A.; Dobhal, M.P.; Mehta, R.; Chen, Y.; Gryshuk, A.; Rittenhouse-Olson, K.; Oseroff, A.; Pandey, R.K. *J. Org. Chem.* **2004**, *69*, 158-172.

[30] Hirohara, S.; Obata, M.; Ogata, S.I., Ohtsuki, C., Higashida, S., Ogura, S.I., Okura, I., Takenaka, M., Ono, H., Sugai, Y. *J. Photochem. Photobiol. B Biol.* **2005**, *78*, 7-15.

[31] Yu, B.; Sun, J. *Chem. Commun.* **2010**, *46*, 4668-4679.

[32] Yu, B.; Sun, J.; Yang, X. *Acc. Chem. Res.* **2012**, *45*, 1227-1236.

[33] Yalagala, R.S.; Mazinani, S.A.; Maddalena, L.A.; Stuart, J.A.; Yan, F.; Yan, H. *Carbohydr. Res.* **2016**, *424*, 15-20.

[34] Uppal, T.; Bhupathiraju, N.V.S.D.K.; Vicente, M.G.H. *Tetrahedron* **2013**, *69*, 4687-4693.

[35] Shivran, N.; Tyagi, M.; Mula, S.; Gupta, P.; Saha, B.; Patro, B.S.; Chattopadhyay, S. *Eur. J. Med. Chem.* **2016**, *122*, 352-365.

[36] Badon, I.W.; Lee, J.; Vales, T.P.; Cho, B.K.; Kim, H.-J. *J. Photochem. Photobiol. A Chem.* **2019**, *377*, 214-219.

[37] Bui, H.T.; Mai, D.K.; Kim, B.; Choi, K.H.; Park, B.J.; Kim, H.J.; Cho, S. *J. Phys. Chem. B* **2019**, *123*, 5601-5607.

[38] Nguyen, M.L.; Kim, H.J.; Cho, B.K. *J. Mater. Chem.* **2018**, *6*, 9802-9810.

[39] Praveen, L.; Saha, S.; Jewrajka, S.K.; Das, *J. Mater. Chem B* **2013**, *1*, 1150-1155.

[40] Crosby, G.A.; Demas, J.N. *J. Phys. Chem.* **1971**, *75*, 991-1024.

[41] Choi, K.-H.; Wang, K.K.; Shin, E.P.; Oh, S.L.; Jung, J.S.; Kim, H.K.; Kim, Y.R. *J. Phys. Chem. C.* **2011**, *115*, 3212-3219.

[42] Park, B.J.; Choi, K.H.; Nam, K.C.; Ali, A.; Min, J.E.; Son, H.; Uhm, H.S.; Kim, H.J.; Jung, J.S.; Choi, E.H. *J. Biomed. Nanotechnol.* **2015**, *11*, 226-

235.

[43] Ruan, Z.; Zhao, Y.; Yuan, P.; Liu, L.; Wang, Y.; Yan, L. *J. Mater. Chem. B* **2018**, *6*, 753-762.

[44] Gao, T.; He, H.; Huang, R.; Zheng, M.; Wang, F.F.; Hu, Y.J.; Jiang, F.L.; Liu, Y. *Dye Pigment* **2017**, *141*, 530-535.

[45] Zhu, S.; Zhang, J.; Vegesna, G.; Luo, F.-T.; Green, S.A.; Liu, H. *Org. Lett*. **2011**, *13*, 438-441.

[46] Vu, T.T.; Dvorko, M.; Schmidt, E.Y.; Audibert, J.F.; Retailleau, P.; Trofimov, B.A.; Pansu, R.B.; Clavier, G.; Méallet-Renault, R. *J. Phys. Chem. C* **2013**, *117*, 5373-5385.

[47] Sun, H..; Dong, X.; Liu, S.; Zhao, Q.; Mou, X.; Yang, H.Y.; Huang, W. *J. Phys. Chem. C*. **2011**, *115*, 19947-19954.

[48] Sun, Y.; Qu, Z.; Zhou, Z.; Gai, L.; Lu, H. *Org. Biomol. Chem.* **2019**, *17*, 3617-3622.

[49] Awuah, S.G.; You, Y. *Rsc Adv*. **2012**, *2*, 11169-11183.

[50] Lower, S.K.; El-Sayed, M.A. *Chem. Rev*. **1966**, *66*, 199-241.

[51] Yuster, P.; Weissman, S.I. *J. Chem. Phys*. **1949**, *17*, 1182-1188.

[52] McGlynn, S.P.; Reynolds, M.J.; Daigre, G.W.; Christodoyleas, N.D. *J. Phys. Chem*. **1962**, *66*, 2499-2505.

[53] Mayeda, E.A.; Bard, A.J. *J. Am. Chem. Soc*. **1973**, *95*, 6223-6226.

[54] Malich, G.; Markovic, B.; Winder, C. *Toxicology* **1997**, *124*, 179-192.

[55] Castano, A.P.; Demidova, T.N.; Hamblin, M.R. *Photodiagnosis Photodyn. Ther*. **2005**, *2*, 91-106.

[56] Kessel, D. *J. Natl. Compr. Cancer. Netw*. **2012**, *10*, 56.

[57] Laville, I.; Pigaglio, S.; Blais, J.C.; Doz, F.; Loock, B.; Maillard, P.; Grierson, D.S.; Blais, J. *J. Med. Chem*. **2006**, *49*, 2558-2567.

[58] Monsigny, M.; Roche, A.-C.; Kieda, C.; Midoux, P.; Obrénovitch, A. *Biochimie* **1988**, *70*, 1633-1649.

[59] Sakuma, S.; Yano, T.; Masaoka, Y.; Kataoka, M.; Hiwatari, K.I.; Tachikawa, H.; Shoji, Y.; Kimura, R.; Ma, H.; Yang, Z. *J. Control.release* **2009**, *134*, 2-10.

[60] Wang, Z.; Wu, P.; He, Z.; He, H.; Rong, W.; Li, J.; Zhou, D.; Huang, Y. *J. Mater. Chem. B*. **2017**, *5*, 7591-7597.

[61] Liu, S.; Huang, Y.; Chen, X.; Zhang, L.; Jing, X. *Biomaterials* **2010**, *31*, 2646-2654.

[62] Hill, E.H.; Pappas, H.C.; Evans, D.G.; Whitten, D.G. *Photochem. Photobiol. Sci*. **2014**, *13*, 247-253.

[63] Juarranz, Á.; Jaén, P.; Sanz-Rodríguez, F.; Cuevas, J.; González, S. *Clin. Transl. Oncol*. **2008**, *10*, 148-154.

[64] Brasseur, N.; Ouellet, R.; La Madeleine, C.; Van Lier, J.E. *Br. J. Cancer* **1999**, *80*, 1533-1541.

[65] Ricchelli, F.; Franchi, L.; Miotto, G.; Borsetto, L.; Gobbo, S.; Nikolov, P.; Bommer, J.C.; Reddi, E. *Int. J. Biochem. Cell Biol*. **2005**, *37*, 306-319.

[66] Zang, L.; Zhao, H.; Hua, J.; Qin, F.; Zheng, Y.; Zhang, Z.; Cao, W. *Dye Pigment* **2017**, *142*, 465-471.

[67] Makhseed, S.; Machacek, M.; Alfadly, W.; Tuhl, A.; Vinodh, M.; Simunek, T.; Novakova, V.; Kubat, P.; Rudolf, E.; Zimcik, P. *Chem. Commun*. **2013**, *49*, 11149-11151.

PART 3

Facile Synthesis of Mitochondria-Targeting Triphenyphosphine-Modified BODIPY Derivatives for Photodynamic Therapy

3.1. Introduction

In spite of the last progress in discerning the biological mechanisms behind cancer progression and the numerous cancer therapies that have been comprehensively developed over the past decades, cancer remains one of the hardest diseases to overcome since the number of cancer patients and its corresponding mortality rate are steadily increasing [1]. A number of challenges are also associated with the conventional use of anticancer agents including drug resistance, toxicity, and frequent relapses [2,3]. Hence, a compelling necessity is emparative in designing alternative cancer therapy that would solve the aforementioned challenges. Photodynamic therapy (PDT) is an emerging cancer treatment that employs a PS that acts like a drug, a molecular oxygen, and a light source of a suitable wavelength [4]. It has gained importance as an alternative cancer therapy due to its noninvasive, low systemic damage, and easy-to-control features [5]. The therapeutic effect of PDT is achieved by initially localizing the PS within the cell or its subcellular compartments and subsequently exciting it by a photon of a suitable wavelength. This process allows the PS to undergo an intersystem crossing (ISC) from its ground state (S_0) to an excited triplet state (T_1). Upon relaxation to the S_0, an energy transfer from

the excited PS to the surrounding molecular oxygen generates highly reactive oxygen species (ROS), mainly singlet oxygen ($^1O_2$), resulting in an irreversible damage to the cancer cells [2,4]

There has been a wide array of PS developed for PDT applications including metal complexes (Ru or Ir), indocyanine-based dyes, boron dipyrromethene (BODIPY) derivatives, and among others [6-11]. In particular, BODIPY derivatives have shown great potentials for PDT use due to its unique spectroscopic and photophysical advantages such as excellent fluorescence quantum yield, extinction coefficient, high chemical stability, and photostability [12-15]. Furthermore, the BODIPY dyes can be straightforwardly synthesized and modified via a wide range of synthetic reactions to tailor fit its intended application. For instance, the ROS generation capabilities of the BODIPY dyes can be significantly improved by incorporating halogen atoms to its core. It is well documented that such attachment of halogen atoms to the BODIPY core has enhanced ISC transitions and consequently the singlet $^1O_2$ quantum yield via heavy atom effect [16]. However, it is worth noting that a successful PDT agent is highly reliant not only to an efficient ROS generation but also to an effective cellular localization. The BODIPY core is highly hydrophobic and lack selectivity to target tumour cells. Hence, functionalization of the BODIPY derivatives that would render them tumor-targeting is highly desirable.

The idea of targeting mitochondrion, a dynamic subcellular organelle, as an avenue for cancer therapy has been emerging due to its crucial roles in various important biological processes including energy production, central metabolism, redox signaling, cellular differentiation, and regulation of the cell cycle and cell growth [4,17-20]. Recent reports indicated that michondrial morphologies and properties were closely correlated with cell functions [21,22]. Particularly, pathological cancer cells exhibited unique mitochondrial characteristics including high ROS and glutathione levels, alkaline pH,

high temperature, and highly negative membrane potential [23,24]. These biological differences between healthy and malignant cells have been exploited as a basis for the design of mitochondrial-targeting therapeutic agents that may preferentially accumulate within the mitochondria of cancer cells [23]. For instance, the highly negative membrane potential of malignant cells enables the selective entry of molecules with delocalized positive charge precisely to the cancer mitochondria [25]. Among the multitude of mitochondria-targeting vector, triphenylphosphonium ion (TPP) has been widely investigated mainly due to its good stability in the biological system, low chemical reactivity toward cellular component, and facile synthesis and purification. Moreover, the hydrophobicity associated with the lipophilic cation of TPP, aside from the charge, facilitates good interactions with the hydrophobic inner mitochondrial membrane resulting to better penetration into the cancer mitochondria [26].

Herein, we report the facile synthesis of a series of mitochondria-targeting BODIPY derivatives with intrinsic photodynamic therapeutic capabilities. The BODIPY meso-position was functionalized with a TPP moiety for mitochondrial targeting while its core was iodinated to improve ROS generation upon irradiation. Extensive photophysical investigations were carried out to the synthesized dyes including fluorescence quantum yield, singlet oxygen quantum yield, and UV/Vis absorbance and emission measurements. Furthermore, the biocompatibilities, mitochondrial-targeted imaging capabilities, and photodynamic therapeutic properties of the synthesized BODIPY derivatives were evaluated against two distinct pathological cancer cell lines (cervical cancer HeLa and breast cancer MCF-7 cell lines).

3.2. Materials and Methods

3.2.1. Chemicals and equipment

All reagents were obtained from commercial sources. Boron trifluoride diethyl etherate ($BF_3 \cdot Et_2O$), 5-bromovaleryl chloride, 2,4-dimethyl pyrrole, triethylamine (TEA), *N*-iodosuccimide (NIS) and triphenylphosphine were purchased from Sigma Aldrich (St. Louis, MO, USA). Sodium hydrogen carbonate ($NaHCO_3$), magnesium sulfate ($MgSO_4$), and ammonium carbonate [$(NH_4)_2CO_3$] were procured from Daejung Chemical (Gyeonggi-do, South Korea) and used without further purification. Ethyl acetate (EtOAc), dichloromethane (CH_2Cl_2), acetronitrile methanol, and other solvents were of analytical grade and were dried under calcium hydride prior to use. All compounds were characterized by ^1H- and ^{13}C-NMR spectroscopy on a Bruker AM 250 spectrometer (Billerica, MA, USA).

3.2.2. Synthesis of TPP-functionalized BODIPY derivatives

2.2.2.1. Synthesis of BODIPY dye 1

The BODIPY dye 1 was synthesized in accord to our previously described procedure [27]. Briefly, 5-bromovaleryl chloride (1.14 mL, 8.52 mmol) and 2,4-dimethyl pyrrole (1.75 mL, 17.04 mmol) were dissolved in dry CH_2Cl_2 (100 mL). The resulting mixture was then degassed with a stream of Ar gas for 2 min, refluxed for 2 h, and the solvents were then evaporated on a rotary evaporator. A mixture of toluene and CH_2Cl_2 (10:1, v/v) was added to the residual mixture, followed by TEA (4.8 mL) and $BF_3 \cdot Et_2O$ (4.2 mL). The mixture was heated

at 50° C for 1.5 h and the solvents were subsequently evaporated. The crude product was purified by column chromatography to obtain the BODIPY dye as an orange solid (2.12 g, 65% yield).

^{1}H-NMR (300 MHz, $CDCl_3$, δ, ppm): 6.07 (s, 2H), 3.48-3.43 (t, 2H), 3.02-2.96 (t, 2H), 2.52 (s, 6H), 2.43 (s, 6H), 2.08- 2.04 (m, 2H), 1.87- 1.82 (m, 2H).

3.2.2.2. Synthesis of BODIPY Dyes 2a and 2b

The BODIPY dyes 2a and 2b were synthesized according to our previously reported procedure [28]. In the case for mono-iodinated BODIPY dye 2a, BODIPY dye 1 (250 mg, 0.65 mmol) was initially dissolved in dried CH_2Cl_2, and added with NIS (73 mg, 0.33 mmol). The resulting mixture was stirred at room temperature for 2 h and the solvents were then evaporated *in vacuo.* The crude product was subjected to column chromatography to obtain BODIPY dye 2a as an orange solid (225 mg, 68% yield).

^{1}H-NMR (300MHz, $CDCl_3$, δ, ppm): δ 6.13 (s, 1H), 3.47-3.43 (t, 2H), 3.01-2.97 (t, 2H), 2.60 (s, 3H), 2.53 (s, 3H), 2.46 (s, 3H), 2.43 (s, 3H), 2.08- 2.03 (m, 2H), 1.84- 1.79 (m, 2H).

The BODIPY dye 2b was afforded in the same procedure as the mono-iodinated BODIPY dye 2a, except that the NIS equivalents were doubled. The BODIPY dye 2b was obtained as a red solid (81% yield).

^{1}H-NMR (300MHz, $CDCl_3$, δ, ppm): δ 3.49-3.44 (t, 2H), 3.08-3.03 (t, 2H), 2.62 (s, 6H), 2.50 (s, 6H), 2.10- 2.05 (m, 2H), 1.86- 1.78 (m, 2H).

3.2.2.3. General procedure for the preparation of TPP-functionalized BODIPY dyes

A series of TPP-functionalized BODIPY dyes BOD-TPP, TPP-I, and TPP-I2 was synthesized [29] and a representative process is described for BOD-TPP.

BOD-TPP: BODIPY dye 1 (55 mg, 0.14 mmol) and triphenylphosphine (113 mg, 0.43 mmol) were dissolved in 30 mL dry acetonitrile. The resulting mixtures was refuxed for 48 h and the solvents were subsequently removed on a rotary evaporator. The residue was purifed by silica gel column chromatography employinh dichloromethane/acetone/methanol (10/2/1) eluent to afford an orange solid (32 mg, 35% yield).

^{1}H-NMR (300 MHz, CDCl3, δ, ppm): δ 8.05 (s, 1H), 6.14 (s, 2H), 4.52-4.5 (t, 2H), 4.44- 4.39 (m, 2H), 3.96- 3.94 (m, 2H), 3.84- 3.78(m, 4H), 3.76- 3.73 (m, 2H), 3.70- 3.67 (m, 4H), 3.61- 3.58 (t, 2H), 3.05- 3.03 (m, 2H), 2.45 (s, 6H), 2.39 (s, 6H), 1.64-1.61 (m, 4H)

^{13}C-NMR (75 MHz, CD30D, δ, ppm): 155.02, 146.86, 145.43, 142.22, 132.39, 125.46, 122.53, 104.87, 103.47, 80.57, 77.02, 76.1, 74.72, 74.38, 72.37, 70.07, 63.2, 62.26, 61.8, 55.03, 50.29, 32.71, 31.33, 30.7, 28.55, 23.64, 16.4, 14.26

TPP-I: The BODIPY dye TPP-I was prepared in accord to the above-detailed general procedure to afford the title product as an orange solid (30% yield).

^{1}H-NMR (300 MHz, CDCl3, δ, ppm): δ 8.03 (s, 1H), 6.21 (s, 1H), 4.45-4.43 (t, 2H), 4.4- 4.39 (m, 2H), 3.97-3.94 (m, 2H), 3.86- 3.81 (m, 4H), 3.75- 3.74 (m, 2H), 3.63- 3.58 (m, 4H), 3.47- 3.46 (t, 2H), 2.88-2.87 (t, 2H), 2.53 (s, 3H), 2.48 (s, 3H), 2.3 (s, 6H), 2.08- 2.07 (m, 2H), 1.56- 1.55 (m, 2H)

^{13}C-NMR (75 MHz, CD3OD, δ, ppm): 164.92, 157.84, 153.67, 146.95, 145.64, 144.75, 141.76, 133.13, 131.89, 125.53, 124.11, 105.05, 103.47, 80.69, 77.0, 76.49, 76.25, 74.74, 72.47, 70.32, 63.1, 62.46, 61.92, 50.71, 31.65, 31.27, 29.52, 28.59, 18.73, 16.74, 14.8

TPP-I2: The BODIPY dye TPP-I2 was synthesized according to the above-detailed general procedure to afford the title product as a red solid (32% yield).

^{1}H-NMR (300 MHz, CDCl3, δ, ppm): δ 8.05 (s, 1H), 4.43- 4.41 (t, 2H), 4.38- 4.36 (m, 2H), 3.91- 3.8 (m, 5H), 3.78- 3.76 (m, 2H), 3.7- 3.66 (m, 5H), 3.47- 3.44 (t, 2H), 3- 2.88 (t, 2H), 2.55 (s, 2H), 2.39 (s, 6H), 2.14- 2.1 (m, 2H), 1.61- 1.59 (m, 2H)

^{13}C-NMR (75 MHz, CD3OD, δ, ppm): 156.35, 147.21, 145.71, 144.12, 132.46, 126.1, 125.53, 105.13, 103.55, 101.87, 98.1, 93.72, 80.63, 77.02, 76.52, 76.28, 74.75, 73.16, 72.62, 71.31, 70.36, 62.47, 61.91, 56.58, 50.3, 32.12, 29.48, 27.8, 23.6, 19.24, 16.35, 14.42

3.2.3. Measurement of photophysical properties

All absorption and steady-state emission spectra were measured at 300-700 nm and repeated at least three times at room temperature. To correct for background intensities, the sample's spectra were subtracted with the spectra of pure solvent measured under identical conditions. UV absorption spectra were collected on a double-beam UV-2800 Uv-vis spectrophotometer (Shimadzu, Kyoto, Japan). The emission spectra were recorded employing a F-4500 steady-state fluorometer (Hitachi, Tokyo, Japan) with an Xenon arc lamp and a photomultiplier detection system.

3.2.4. Fluorescence quantum yield measurements

To obtain the relative fluorescence quantum yields of the synthesized BODIPY dyes, the area under the corrected emission spectrum of the samples were compared with that of a standard solution whose fluorescence quantum yield is known. Rhodamine 6G (Φ_R = 0.94 in methanol) was used as the reference standard [30]. The Φ_S was calculated according to equation 1:

$$\Phi_S = \Phi_R \left(\frac{Grad_S}{Grad_R}\right)\left(\frac{n_S}{n_R}\right)^2$$

where the subscripts S and R denote the tested sample and reference, respectively. In addition, Grad and n represent the gradient of the filled slope and the refractive index of the test solvent used, respectively. The solutions were optically diluted to avoid inner filter effects [31].

3.2.5. Singlet oxygen quantum yield measurements

A chemical quencher, 1,3-diphenylisobenzofuran (DBPF), was used to study the singlet oxygen (Φ_Δ) quantum yields of the synthesized dyes [32]. A mixture of DPBF (absorption ~1.0 at 424 nm in EtOH) and each of the BODIPY dye (absorption ~0.06 at 524 nm in EtOH) was briefly irradiated with a green LED lamp (λ_{max} = 500 nm). Then, photodegradation of DPBF was spectroscopically monitored at 424 nm between 0 and 70 min, depending on the efficiency of the BODIPY dye. Moreover, the singlet oxygen quantum yield was calculated employing the reference hematoporphyrin (HP) (0.53 in ethanol), in accord to the following equation:

$$\Phi_\Delta^S = \frac{k_S}{k_R} \times \Phi_\Delta^R$$

where subscripts S and R represent the sample and reference, respectively, while k represents the slope of the photodegradation rate.

3.2.6. Cells and cell cultures

MCF-7 (human breast adenocarcinoma) and HeLa (human cervix adenocarcinoma) were obtained from the Korean Cell Line Bank. The cells were maintained in RPMI 1640 medium (Gibco, Carlsbad, CA, USA) supplemented with 10% heat-inactivated fetal bovine serum (FBS) and antibiotics (100 U/mL penicillin and 100 mg/mL streptomycin) (WELGENE Inc., Gyeongsangbuk-do, Korea) at 37 ºC in a humidified 5% CO_2 incubator.

3.2.7. Cell proliferation assay

The MCF-7 and HeLa (2×10^3 cells/well) were seeded in 96-well plates. After the cells were maintained for 24 h, cells were treated with the BODIPY dyes at different concentrations for 24 h [33,34]. A cell proliferation assay was measured using CellTiter 96® AQueous One Solution Cell Proliferation Assay (Promega, Madison, WI, USA) according to the manufacturer's instruction. The absorbance was determined at 490 nm using ELISA plate reader (Thermo Fisher Scientific, Inc., Waltham, MA, USA).

3.2.8. Photodynamic anticancer activity assessment

The MCF-7 and HeLa cells were plated at 2×10^3 cells/well in a 96-well plate and incubated at 37 ° C in 5 % CO_2 for 24 h. Then, the cells were treated with the BODIPY dye and further incubated for 2 h at 37 ° C in 5 % CO_2 under dark conditions. After 2 h incubation, the media in all plates were changed with phenol-red free RPMI 1640 media and all cells were irradiated with a green light-emitting diode (LED), which had a wavelength of 530 nm (80%, 10min). Irradiation power of LED was about 9 mW. All cells were then incubated for further 24 h and the cell proliferation was measured using CellTiter 96® AQueous One Solution Cell Proliferation. The assay used was the same method for the cytotoxicity described above.

3.2.9. Morphological assessment of active mitochondria by fluorescent imaging

The MCF-7 and HeLa cells were treated with the BODIPY dye sample (1 μM) for 24 h. Cells were then incubated with a fluorescent probe (MitoTracker Red FM, Invitrogen) for labeling active mitochondria for 45 min. Next, cells were fixed with 4% paraformaldehyde for 10 min and permeabilized for 10 min with 0.1% Triton X-100. Cell nuclei were counterstained with 4′,6-diamidino-2-phenylindole (DAPI) for 1 h at room temperature. Lastly, cells were observed using confocal microscopy (LSM-700, Carl Zeiss, Germany).

3.2.10. Statistical Analysis

All data are expressed as the means ± standard deviations and were compared by one-way analysis of variance and Tukey's test, using Prism GraphPad 6 software (San Diego, CA, USA). Group means were considered as significantly different at $p < 0.05$.

3.3. Results and Discussion

3.3.1. Design and synthesis of TPP-functionalized BODIPY derivatives

The synthesis of the TPP-functionalized BODIPY derivatives was outlined in Scheme 3.1. Firstly, under acid catalysis, the condensation reaction of 2,4-dimethylpyrrole with 5-bromovaleryl chloride was allowed to take place. This was subsequently followed by the treatment with boron trifluoride diethyl etherate in the presence of triethylamine to afford BODIPY 1 in yield of 65%. Then, BODIPY intermediates 2a and 2b were obtained by treating BODIPY 1 with N-iodosuccinimide (NIS) in 68 and 81% yields, respectively. Lastly, BODIPYs 2a and 2b were respectively treated with TPP to attain the mitochondria-targeting BODIPY derivatives (TPP-I and TPP-I2, respectively). A control non-iodinated dye, BOD-TPP, was also synthesized by directly reacting BODIPY 1 with TPP. The structures of all TPP-functionalized BODIPY derivatives and their corresponding intermediates were confirmed by ^{1}H-NMR spectroscopy, while additional ^{13}C-NMR and mass spectroscopic characterizations were done for the last three BODIPY dyes, BOD-TPP, TPP-I, and TPP-I2.

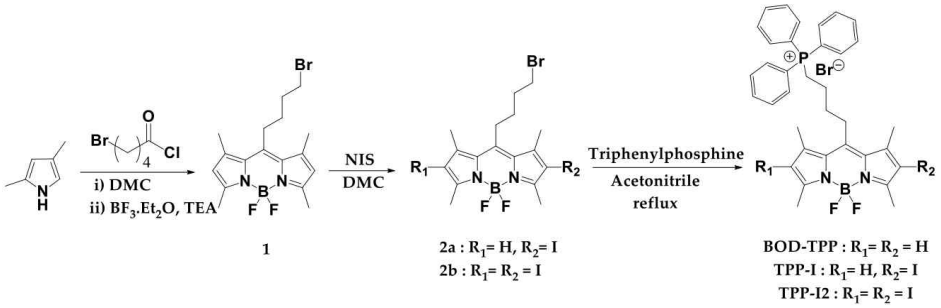

Scheme 3.1. Synthesis of the mitochondria-targeting and TPP-functionalized BODIPY dyes.

3.3.2. Singlet oxygen generation of TPP-functionalized BODIPY derivatives

The success of a PDT agent highly relies on its ability to effectively undergo singlet-to-triplet ISC and efficiently generate singlet oxygen ($^1O_2$)to induce irreversible damage to the cancer cells. However, majority of BODIPY-based PSs exhibit low singlet oxygen quantum yields since an intramolecular electronic transition from a singlet to a triplet excited state is spin-forbidden [11]. It generally requires a spin-orbit perturbation in order for an effective transition between states of different spin multiplicities to take place [35]. Such spin-orbit perturbation could be achieved by directly incorporting heavy atoms like halogens onto the PS or confining the molecule within a heavy-atom-rich environment [36,37]. Herein, the BODIPY core was iodinated at 2- and 2,6-positions and their respective 102 generation capabilities were compared to that of the uniodinated control, which depends exclusively on its intrinsic spin-orbit coupling capability in this process. Moreover, a specific 102 quencher, 1,3-diphenylisobenzofuran (DPBF), was employed to assess the efficiency of the $^1O_2$ generation of the synthesized BODIPY derivatives. The basis for the indirect detection of $^1O_2$ is the ability of DPBF to react with $^1O_2$ and form endoperoxides via a 1,4-cycloaddition reaction. The generated endoperoxides subsequently decay to 1,2-dibenzoylbenzene, causing in the total collapse of its extended π-electron system and its typical spectroscopic properties [38]. Hence, the change in the absorption bands of DPBF was monitored at 424 nm to track spectroscopically the photooxidation rates of the quencher [32]. As shown in Figure 3.1a, there was no significant change in the absorbance of DPBF even after LED irradiation (λmax = 500 nm, 9 mW/cm^2) for 40 min, demonstrating the chemical stability of DPBF under the indicated excitation conditions. On the other hand, incubation of DPBF with the mono- and diiodinated BODIPY dyes, TPP-I and TPP-I2, respectively, and subsequent LED irradiation resulted to an extensive photodegradation of

the DPBF. This was evidently manifested disappearance of its distinct absorbance band in the region of 424 nm. Although the diiodinated dye TPP-I2 showed a more abrupt disappearance of the DPBF absorbance band (~6 min, Fig. 3.1c), when compared to that of the monoiodinated dye TPP-I (~10 min, Fig. 3.1b).

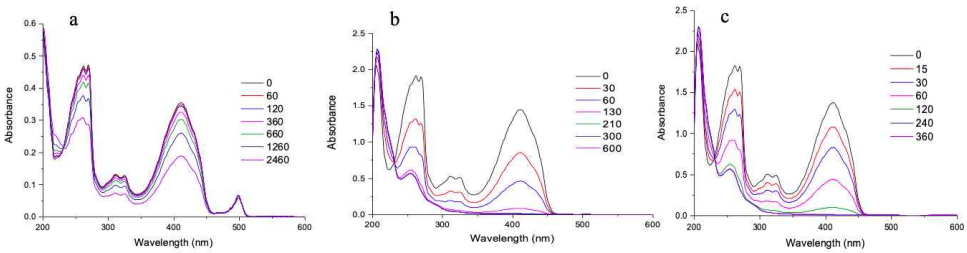

Figure 3.1. Time-dependent absorption spectra of 1,3-diphenylisobenzofuran (DPBF) in EtOH with (a) BOD-TPP, (b) TPP-I, and (c) TPP-I2 after LED light excitation at 500 nm.

To quantify the $^1O_2$ quantum yields (Φ_Δ) of the TPP-functionalized BODIPY dyes, hematoporphyrin (HP) was used as a reference standard whose Φ_Δ is known (0.53 in EtOH). The decay curves of the absortion density of DPBF in the presence of the test samples and HP were respectively obtained and their degradation rates for were linearly fitted. The non-iodinated control, BOD-TPP, did not generate $^1O_2$ (Φ_Δ = 0.01), while iodinated BODIPY derivatives showed elevated $^1O_2$ generation under LED irradiation. The Φ_Δ of the BODIPY dyes TPP-I and TPP-I2 were found to be 0.36 and 0.87, respectively. The additional heavy iodine atom in the case of TPP-I2 induced further spin-orbit perturbations, leading to a faster diminishing rate of DPBF absorbance bands and the higher singlet oxygen quantum yield, compared to that of the monoiodinated counterpart. Nonetheless, both iodinated BODIPY dyes displayed the heavy atom effect and generated adequate amount singlet oxygen, showcasing their potentials as viable photodynamic therapeutic agents for cancer treatment.

3.3.3. Photodynamic anticancer activity of the TPP-functionalized BODIPY derivatives

The cytotoxicities in the dark of the TPP-functionalized BODIPY derivatives was assessed by incubating the synthesized dyes at a concentration range from 0 to 20 nM into two distinct pathological cancer cell lines (cervical cancer HeLa and breast cancer MCF-7 cell lines) and measuring their respective cell viabilities without LED irradiation via a standard [3-(4,5-dimethylthiazol-2-yl)-5-(3-carboxymethoxyphenyl)-2-(4-sulfophenyl)-2H-tetrazolium] (MTS) assay. In any metabolically active cells, the tetrazolium MTS compounds are reduced to formazan by the mitochondrial succinate dehydrogenase enzymes. The amount of formazan formed can be measured spectroscopically at 490 nm and is directly proportional to the number of living cells in culture [39].

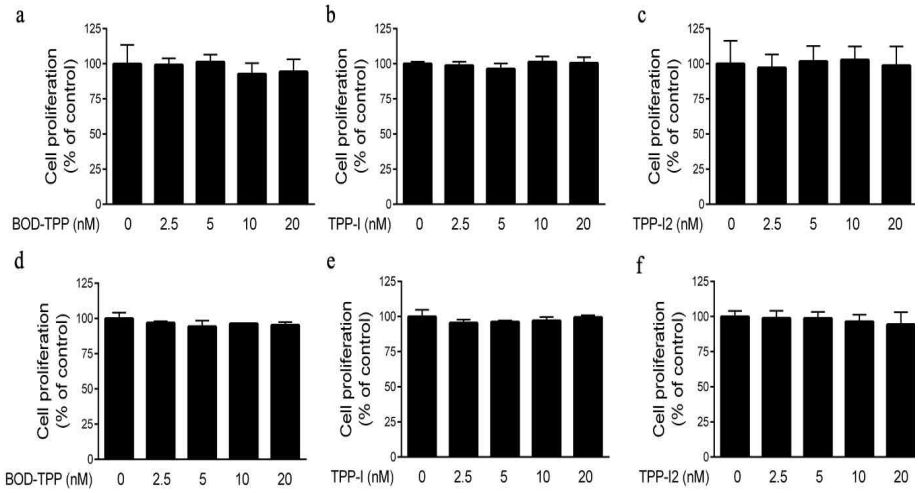

Figure 3.2. Cell survival rates of MCF-7 cells after treatment with (a) BOD-TPP, (b) TPP-I, and (c) TPP-I2; cell survival rates of HeLa cells after treatment with (d) BOD-TPP, (e) TPP-I, and (f) TPP-I2 under dark conditions.

As shown in Figure 3.2, the TPP-functionalized BODIPY derivatives evidently exhibit no obvious toxicity towards carcinoma cell lines across all concentrations. All BODIPY dyes showed no significant toxicities in the dark against HeLa, and at least 95% of the cell were viable even at a maximum dye concentration of 20 nM. Furthermore, MCF-7 cell lines exhibited the same trends of low toxicities in the dark, wherein at least 92% of the cells are retained even after incubation at a maximum concentration (20 nM). The results demontrated that the TPP-functionalized BODIPY derivatives exhibited favorable biocompatibilities without incurring any significant cytotoxicities in the dark against HeLa and MCF-7 and could be attributed to the good biocompatibility of the TPP moiety.

To further evaluate the photodynamic therapeutic potential of the synthesized dyes, the cancer cell lines that were incubated with various concentrations BODIPY dyes were subjected to LED irradiation at 530 nm for 10 min ($9mW/cm^2$) and cell proliferation were determined using the same MTS assay. As indicated in Figure 3.3, there were no significant cytotoxicities observed against HeLa and MCF-7 cancer cell lines for the uniodinated control, BOD-TPP, even after LED irradiation for 10 min. On the other hand, a significant dose-dependent cytotoxicities ($p<0.05$) to the two cancer cell lines was observed for both iodinated-BODIPY derivatives, which could be attributed to the heavy atom effect and subsequently effective 102 generation induced by the incorporated iodine atoms. Both TPP-I and TPP-I2 has induced significant cytotoxic effects to both HeLa and MCF-7 cells even at the lowest concentartion employed (2.5 nM), and the severity of the toxic effects was more prominent at higher dye concentrations. Furthermore, di-iodinated BODIPY dye, TPP-I2, has shown superior cytotoxicities against both cancer cells when compared to its mono-iodinated counterpart, TPP-I, across all concentrations used. For instance, at 20 nM, the HeLa cell viability significantly dropped to 34.8% and 7.0% after incubation with TPP-I and TPP-I2, respectively. The same cytotoxic trends were found for MCF-7 cells in which the cell viability has plummeted significantly to 48.8% and 10.0% after incubation with TPP-I and TPP-I2, respectively, at 20 nM dye concentration.

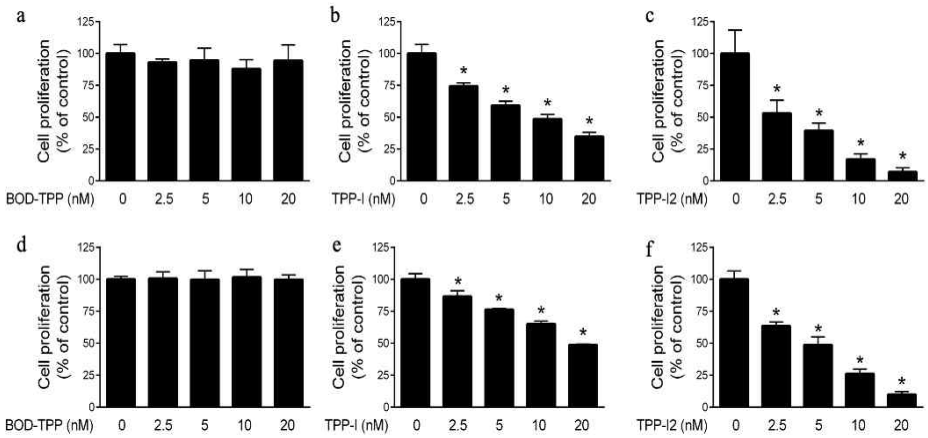

Figure 3.3. Dose-dependent cytotoxicities of synthesized BODIPYs. Cell survival rates of MCF-7 cells after treatment with (a) BOD-TPP, (b) TPP-I, and (c) TPP-I2; cell survival rates of HeLa cells after treatment with (d) BOD-TPP, (e) TPP-I, and (f) TPP-I2 under LED light irradiation at 530 nm. *$p < 0.05$ compared to control (0 nM).

3.3.4. Morphological assessment of active mitochondria by fluorescent imaging

To demonstrate the bioimaging capabilities of the TPP-functionalized BODIPY dyes in HeLa and MCF-7 cells, morphological assessment of active mitochondria by fluorescent imaging was conducted using confocal laser scanning microscopy (CLSM). As shown in Fig. 3.4, uniodinated control BOD-TPP demonstrated a bright green fluorescence in both HeLa and MCF-7 cells, which could be attributed to its high fluorescence quantum yield. Furthermore, it can be observed that the green fluorescence of BOD-TPP has perfectly overlapped with the red flourescence of Mito Tracker Red (Fig. 3.5), suggesting that the dye has been successfully taken in by the cells and efficiently localized, partly due to mitochondrial-targeting capability of the TPP moiety. The iodinated

BODIPY derivatives, TPP-I and TPP-I2, have also displayed green flourescence in both HeLa and MCF-7 cells albeit slightly quenched. The quenching of their flourencence intensities could be attributed to the heavy atom effect of the incorporated halogen. Nevertheless, the results indicated that the TPP-functionalized BODIPY dyes can be viable material for fluorescence bioimaging due to their efficient localization into the cells while exhibiting good fluorescence upon excitation.

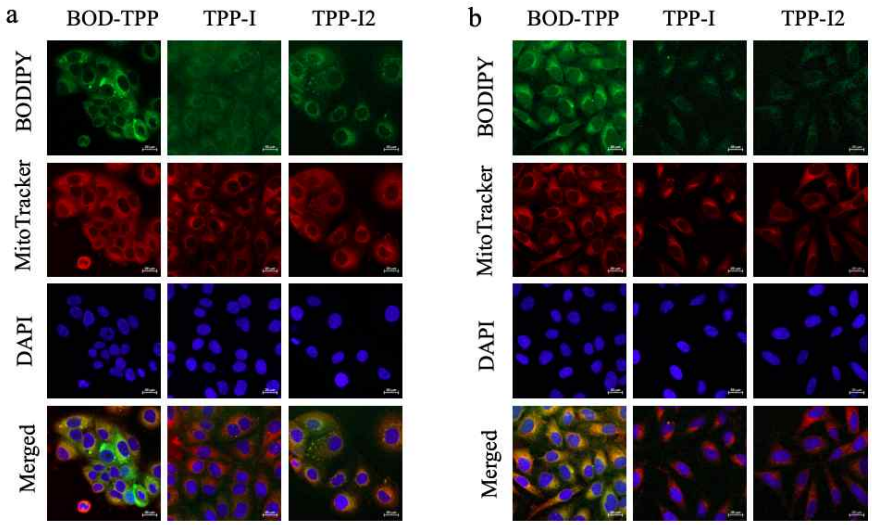

Figure 3.4. CLSM images of (a) MCF-7 human breast and (b) HeLa cervical cancer cells with the sythesized BODIPY dyes (concentration = 1.0 μM).

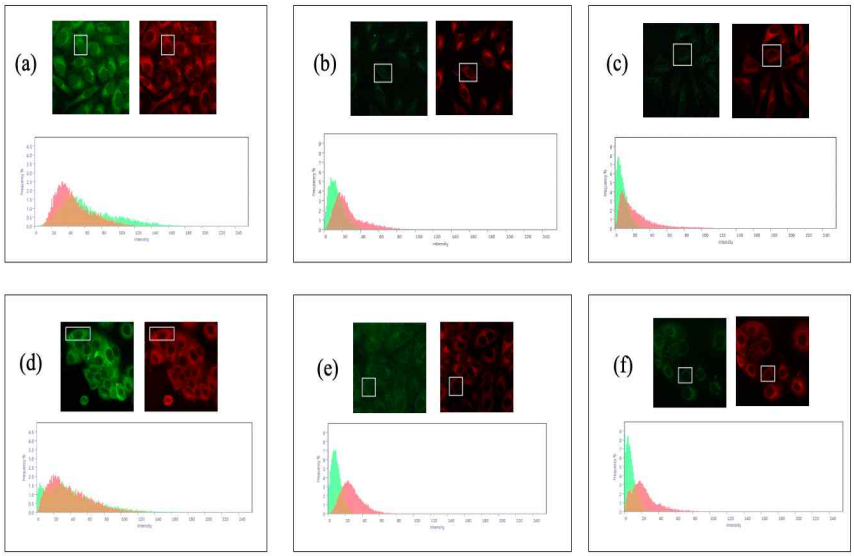

Figure 3.5. Fluorescence spectral overlap between Mito Tracker and (a) BOD-TPP, (b) TPP-I, and (c) TPP-I2 in HeLa cells; fluorescence spectral overlap between Mito Tracker and (a) BOD-TPP, (b) TPP-I, and (c) TPP-I2 in MCF-7 cells.

3.4. Conclusions

Herein, we reported the synthesis of the TPP-functionalized BODIPY derivatives and investigated their photodynamic therapeutic properties and mitochondria-targeted bioimaging capabilities in two carcinoma cell lines. The halogenated BODIPY derivatives have demonstrated efficient generation of single oxygen species than the uniodinated control. All of the synthesized BODIPY derivatives exhibited excellent biocompability and induced no significant cytotoxicities to the two tested cancer cell lines (HeLa and MCF-7) in the absence of LED irradiation. Moreover, incubation of the cancer cell lines with the halogenated dyes, when compared to that of the uniodinated control,

resulted in a significant decrease in the cell viabilities after LED irradiation. The BODIPY dyes have also exhibited good cell bioimaging capabilities, partly due to mitochondrial-targeting capability of the TPP moiety. Overall, the results presented herein demonstrate a facile synthetic route to the TPP-functionalized BODIPY-based PS and show the potentials of these synthesized dyes as effective photosensitizers for photodynamic cancer therapy.

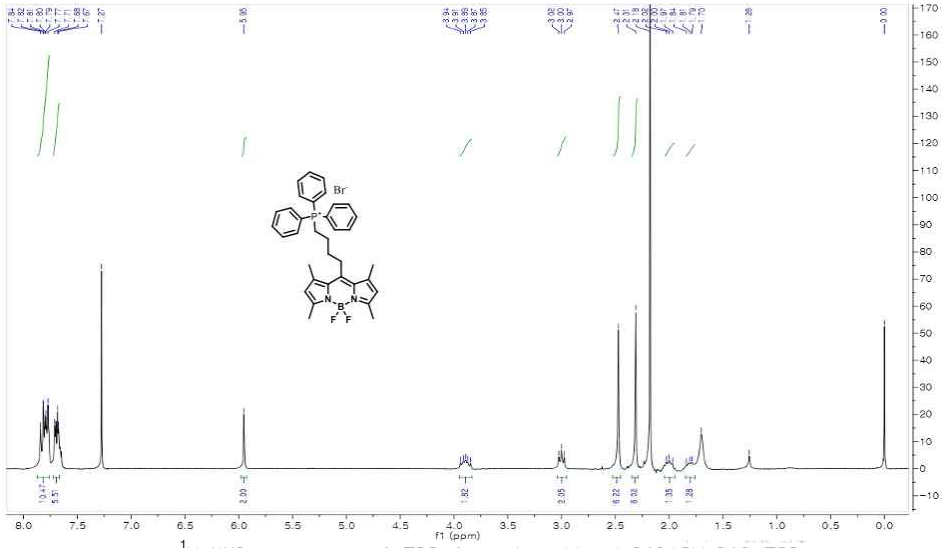

^{1}H-NMR spectrum of TPP-functionalized BODIPY BOD-TPP.

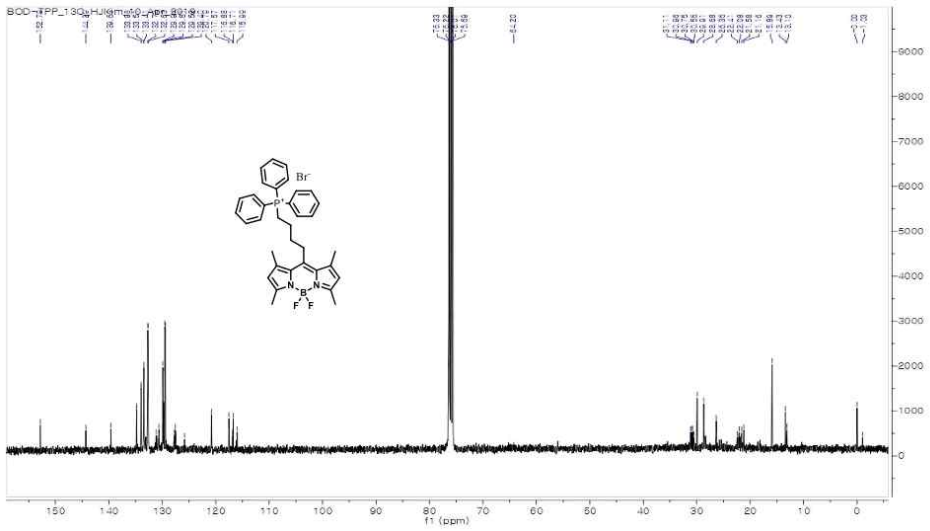

^{13}C-NMR spectrum of TPP-functionalized BODIPY BOD-TPP.

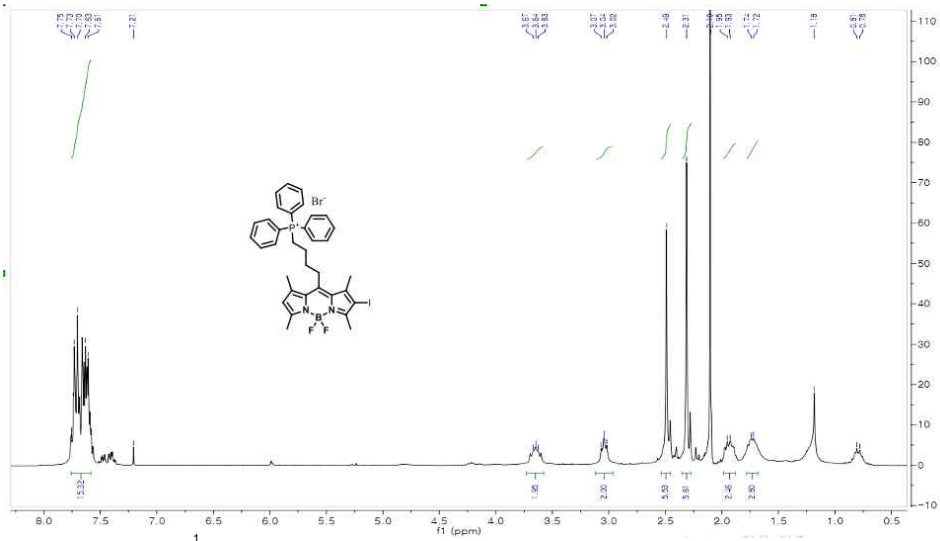

^{1}H-NMR spectrum of TPP-functionalized BODIPY TPP-I.

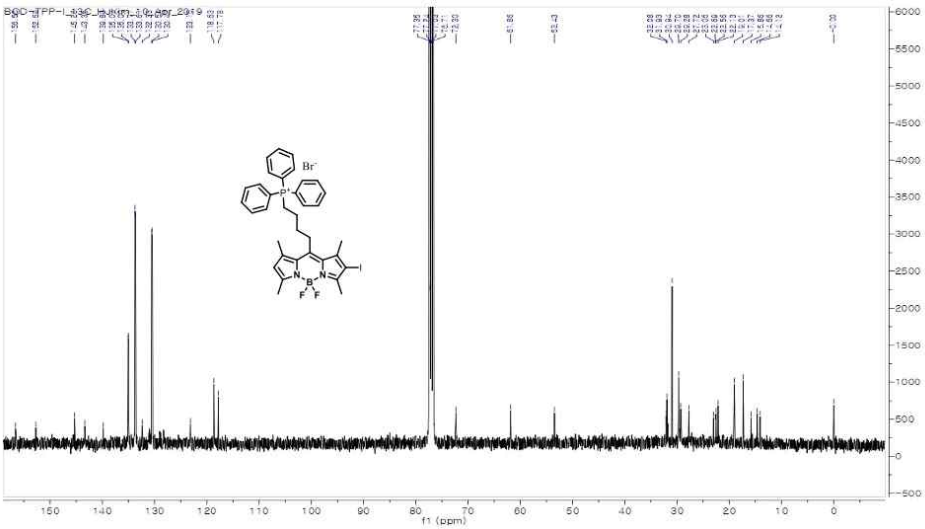

^{13}C-NMR spectrum of TPP-functionalized BODIPY TPP-I.

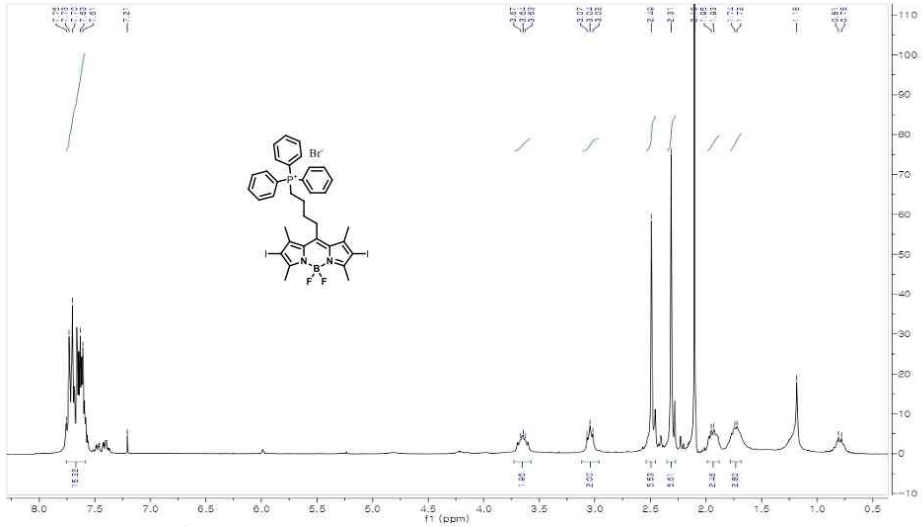

^{1}H-NMR spectrum of TPP-functionalized BODIPY TPP-I2.

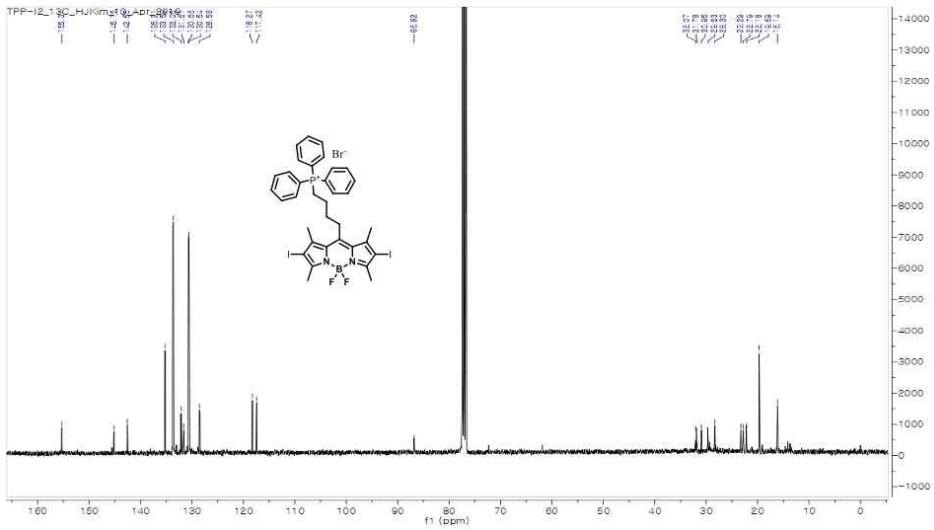

^{13}C-NMR spectrum of TPP-functionalized BODIPY TPP-I2.

3.5. References

[1] Bray, F.; Ferlay, J.; Soerjomataram, I.; Siegel, R.L.; Torre, L.A.; Jemal, A., *CA: a cancer journal for clinicians*, **2018**, *68*, 394-424.

[2] Dolmans, D.E.; Fukumura, D.; Jain, R.K. *Nature reviews cancer*, **2003**, *3*, 380-387.

[3] Noh, I.; Kim, H.O.; Choi, J.; Choi, Y.; Lee, D.K.; Huh, Y.M.; Haam, S., *Biomaterials*, **2015**, *53*, 763-774.

[4] Jeena, M.T.; Kim, S.; Jin, S.; Ryu, J.H., *Cancers*, **2020**, *12*, 4.

[5] Cai, Y.; Tang, Q.; Wu, X.; Si, W.; Zhang, Q.; Huang, W.; Dong, X., *ACS Applied Materials & Interfaces*, **2016**, *8*, 10737-10742.

[6] Zhang, L.; Li, Y.; Che, W.; Zhu, D.; Li, G.; Xie, Z.; Song, N.; Liu, S.; Tang, B.Z.; Liu, X.; Su, Z. *Advanced Science*, **2019**, *6*, 1802050.

[7] Shi, G.; Monro, S.; Hennigar, R.; Colpitts, J.; Fong, J.; Kasimova, K.; Yin, H.; DeCoste, R.; Spencer, C.; Chamberlain, L.; Mandel, A., *Coordination Chemistry Reviews*, **2015**, *282*, 127-138.

[8] Urbanska, K.; Romanowska-Dixon, B.; Matuszak, Z.; Oszajca, J.; Nowak-Sliwinska, P.; Stochel, G. *Acta Biochimica Polonica,* **2002**, *49*, 387-391.

[9] Otani, A.; Sasahara, M.; Yodoi, Y.; Aikawa, H.; Tamura, H.; Tsujikawa, A.; Yoshimura, N. *American journal of ophthalmology*, **2007**, 144, 7-14.

[10] Yang, Y.; Guo, Q.; Chen, H.; Zhou, Z.; Guo, Z.; Shen, Z. *Chemical communications*, **2013**, *49*, 3940-3942.

[11] Awuah, S.G.; You, Y. *Rsc Advances*, **2012**, *2*, 11169-11183.

[12] Kamkaew, A.; Burgess, K. *Journal of medicinal chemistry*, **2013**, *56*, 7608-7614.

[13] Sun, T.; Guan, X.; Zheng, M.; Jing, X.; Xie, Z. *ACS medicinal chemistry letters,* **2015**, *6*, 430-433.

[14] He, H.; Lo, P.C.; Yeung, S.L.; Fong, W.P.; Ng, D.K. *Chemical Communications*, **2011**, *47*, 4748-4750.

[15] Kolemen, S.; Işık, M.; Kim, G.M.; Kim, D.; Geng, H.; Buyuktemiz, M.; Karatas, T.; Zhang, X.F.; Dede, Y.; Yoon, J.; Akkaya, E.U. A*ngewandte Chemie*, **2015**, *127*, 5430-5434.

[16] Gorman, A.; Killoran, J.; O'Shea, C.; Kenna, T.; Gallagher, W.M.; O'Shea, D.F. *Journal of the American Chemical Society,* **2004**, *126*, 10619-10631.

[17] Hoye, A.T.; Davoren, J.E.; Wipf, P.; Fink, M.P.; Kagan, V.E. A*ccounts of chemical research*, **2008**, *41*, 87-97.

[18] Wang, X.; Peralta, S.; Moraes, C.T. Academic Press, In *Advances in cancer research*, **2013**, *119*, 127-160.
[19] Wallace, D.C. *Nature Reviews Cancer*, 2012, *12*, 685-698.
[20] He, H.; Li, D.W.; Yang, L.Y.; Fu, L.; Zhu, X.J.; Wong, W.K.; Jiang, F.L.; Liu, Y., *Scientific reports*, **2015**, *5*, 13543.
[21] Karbowski, M.; Youle, R.J., *Cell Death & Differentiation*, **2003**, *10*, 870-880.
[22] Dodani, S.C.; Leary, S.C.; Cobine, P.A.; Winge, D.R.; Chang, C.J. J*ournal of the American Chemical Society*, 2011, *133*, 8606-8616.
[23] Battogtokh, G.; Cho, Y.Y.; Lee, J.Y.; Lee, H.S.; Kang, H.C. F*rontiers in pharmacology*, 2018, *9*, 922.
[24] Cho, H.; Cho, Y.Y.; Shim, M.S.; Lee, J.Y.; Lee, H.S.; Kang, H.C. *Biochimica et Biophysica Acta (BBA)-Molecular Basis of Disease*, **2020**, 165808.
[25] Zorova, L.D.; Popkov, V.A.; Plotnikov, E.Y.; Silachev, D.N.; Pevzner, I.B.; Jankauskas, S.S.; Babenko, V.A.; Zorov, S.D.; Balakireva, A.V.; Juhaszova, M.; Sollott, S.J., *Analytical biochemistry*, **2018**, *552*, 50-59.
[26] Zielonka, J.; Joseph, J.; Sikora, A.; Hardy, M.; Ouari, O., Vasquez-Vivar, J.; Cheng, G.; Lopez, M.; Kalyanaraman, B., *Chemical reviews*, **2017**, *117*, 10043-10120.
[27] Badon, I.W.; Lee, J.; Vales, T.P.; Cho, B.K.; Kim, H.J. *Journal of Photochemistry and Photobiology A: Chemistry*, **2019**, *377*, 214-219.
[28] Squeo, B.M.; Pasini, M. *Supramolecular Chemistry*, **2020**, *32*, 56-70.
[29] Cheng, G.; Fan, J.; Sun, W.; Sui, K.; Jin, X.; Wang, J.; Peng, X. *Analyst*, **2013**, *138*, 6091-6096.
[30] Praveen, L.; Saha, S.; Jewrajka, S.K.; Das, A. J*ournal of Materials Chemistry B*, **2013**, *1*, 1150-1155.
[31] Crosby, G.A.; Demas, J.N. *The Journal of Physical Chemistry*, **1971**, *75*, 991-1024.
[32] Choi, K.H.; Wang, K.K.; Shin, E.P.; Oh, S.L.; Jung, J.S.; Kim, H.K.; Kim, Y.R. *The Journal of Physical Chemistry C*, **2011**, *115*, 3212-3219.
[33] Park, B.J.; Choi, K.H.; Nam, K.C.; Ali, A.; Min, J.E.; Son, H.; Uhm, H.S.; Kim, H.J.; Jung, J.S.; Choi, E.H. J*ournal of Biomedical Nanotechnology*, **2015**, *11*, 226-235.
[34] Ruan, Z.; Zhao, Y.; Yuan, P.; Liu, L.; Wang, Y.; Yan, L. *Journal of Materials Chemistry B*, **2018**, *6*, 753-762.
[35] Lower, S.K.; El-Sayed, M.A. *Chemical Reviews*, **1966**, *66*, 199-241.
[36] Yuster, P.; Weissman, S.I. *The Journal of Chemical Physics*, **1949**, *17*, 1182-1188.

[37] McGlynn, S.P.; Reynolds, M.J.; Daigre, G.W.; Christodoyleas, N.D. *The Journal of Physical Chemistry*, **1962**, *66*, 2499-2505.

[38] Mayeda, E.A.; Bard, A.J. *Journal of the American Chemical Society*, **1973**, *95*, 6223-6226.

[39] Malich, G.; Markovic, B; Winder, C. *Toxicology*, **1997**, *124*, 179-192.